Earth's Future

RESEARCH ARTICLE
10.1029/2023EF003701

Special Section:
Climate Change, Global Air Quality, and Society

Increased Summer European Heatwaves in Recent Decades: Contributions From Greenhouse Gases-Induced Warming and Atlantic Multidecadal Oscillation-Like Variations

Binhe Luo[1], Dehai Luo[2,3], Wenqing Zhuo[4], Cunde Xiao[1], Aiguo Dai[5], Ian Simmonds[6], Yao Yao[2], Yina Diao[4], and Tingting Gong[7,8]

[1]State Key Laboratory of Earth Surface Processes and Resource Ecology, Beijing Normal University, Beijing, China, [2]Key Laboratory of Regional Climate-Environment for Temperate East Asia, Institute of Atmospheric Physics, Chinese Academy of Science, Beijing, China, [3]University of Chinese Academy of Sciences, Beijing, China, [4]College of Oceanic and Atmospheric Sciences, Ocean University of China, Qingdao, China, [5]Department of Atmospheric and Environmental Sciences, State University of New York, Albany, NY, USA, [6]School of Geography, Earth and Atmospheric Sciences, University of Melbourne, Melbourne, VIC, Australia, [7]CAS Key Laboratory of Ocean Circulation and Waves, Institute of Oceanology, Chinese Academy of Sciences, Qingdao, China, [8]Pilot National Laboratory for Marine Science and Technology (Qingdao), Qingdao, China

Key Points:

- Severe summer heatwaves frequently occurred in central and eastern Europe and western Russia in recent decades
- The greenhouse gases-induced warming and the positive phase of Atlantic Multidecadal Oscillation favor increased European heatwaves
- The increased quasi-stationarity, persistence, zonal scale, and slow decay of the European blocking and Ural blocking favor increased duration, extent and intensity of the European heatwaves

Supporting Information:

Supporting Information may be found in the online version of this article.

Correspondence to:

D. Luo and C. Xiao,
ldh@mail.iap.ac.cn;
cdxiao@bnu.edu.cn

Citation:

Luo, B., Luo, D., Zhuo, W., Xiao, C., Dai, A., Simmonds, I., et al. (2023). Increased summer European heatwaves in recent decades: Contributions from greenhouse gases-induced warming and Atlantic Multidecadal Oscillation-like variations. *Earth's Future*, *11*, e2023EF003701. https://doi.org/10.1029/2023EF003701

Received 6 APR 2023
Accepted 15 JUL 2023
Corrected 16 AUG 2023

This article was corrected on 16 AUG 2023. See the end of the full text for details.

Abstract Summer heatwaves over Europe, which can cause many deaths and severe damage, have become increasingly frequent over central and eastern Europe and western Russia in recent decades. In this paper, we estimate the contributions of the warming due to increased greenhouse gases (GHG) and nonlinear variations correlated with the Atlantic Multidecadal Oscillation (AMO) to the observed heatwave trend over Europe during 1980–2021, when the GHG-induced warming over Europe exhibits a linear trend. It is found that GHG-induced warming contributes to ~57% of the European heatwave trend over 1980–2021, while the cold-to-warm phase shift of the AMO-like variations accounts for ~43% of the trend via the intensification of midlatitude North Atlantic jet. The recent trend of heatwaves over western and northern Europe is mainly due to GHG-induced warming, while that over central and eastern Europe and western Russia is primarily related to the combined effect of the AMO-like variations and GHG-induced warming. To some extent, GHG-induced warming is an amplifier of the increasing trend of recent AMO-related European heatwaves. Moreover, European blocking (Ural blocking, UB) is shown to contribute to 55% (42%) of the AMO-related heatwave trend via the influence of midlatitude North Atlantic jet. In the presence of a strong North Atlantic jet during the recent warm AMO phase, UB events concurrent with positive-phase North Atlantic Oscillation can cause intense, persistent and widespread heatwaves over Europe such as that observed in the summer of 2022.

Plain Language Summary In recent decades, severe summer heatwaves frequently occurred in Eurasia and North America. However, what leads to the increased European heatwaves in recent decades is still debated. In this paper, we quantify the contributions of greenhouse gases (GHG)-induced warming and the multidecadal variations correlated with the Atlantic Multidecadal Oscillation (AMO) to increased European heatwaves in recent decades by assuming that GHG-induced warming shows a linear upward trend. It is revealed that GHG-induced warming contributes to ~57% of the recent European heatwave trend during 1980–2021, whereas the cold-to-warm transition of the AMO-like variations contributes to ~43% of the trend via strengthening the midlatitude North Atlantic jet. In particular, European blocking (EB) (Ural blocking, UB) accounts for ~55% (42%) of the AMO-related heatwave trend, even though the area extent and intensity of European heat waves depend strongly on whether the EB or UB is concurrent with the positive phase of NAO and whether the midlatitude North Atlantic jet is strong.

1. Introduction

In recent decades, summer heatwaves had frequently occurred over Europe (Barriopedro et al., 2011; Fischer & Schar, 2010; Meehl & Tebaldi, 2004) and they show a significant increasing trend over central Europe during 2002–2014 (Johnson et al., 2018) and western Europe during 1979–2020 (Rousi et al., 2022). Recent examples include summer heatwaves occurring over western Europe in 2003 (Black et al., 2004; Stott et al., 2004), western Russia in 2010 (Dole et al., 2011; Schneidereit et al., 2012), central Europe in 2015 (Mecking et al., 2019) and 2018 (Li et al., 2020), and the widespread heatwaves over Europe in the summer of 2022. The frequently

Author Contributions:

Conceptualization: Binhe Luo, Dehai Luo, Cunde Xiao, Aiguo Dai, Ian Simmonds
Data curation: Binhe Luo
Formal analysis: Binhe Luo, Dehai Luo, Wenqing Zhuo
Funding acquisition: Binhe Luo, Dehai Luo
Investigation: Binhe Luo
Methodology: Binhe Luo, Dehai Luo, Wenqing Zhuo
Project Administration: Binhe Luo, Dehai Luo
Resources: Binhe Luo
Software: Binhe Luo
Supervision: Binhe Luo, Dehai Luo, Cunde Xiao, Yina Diao, Tingting Gong
Validation: Binhe Luo, Dehai Luo
Visualization: Binhe Luo, Wenqing Zhuo
Writing – original draft: Binhe Luo
Writing – review & editing: Binhe Luo, Dehai Luo, Cunde Xiao, Aiguo Dai, Ian Simmonds, Yao Yao

occurring severe summer heatwaves with persistent high temperatures have large impacts on human health, regional economies, ecosystems and societies (Vandentorren et al., 2004). For example, the European heatwaves in 2003 and 2010 may have led to 30,000 and 56,000 deaths, respectively (Dole et al., 2011; Trigo et al., 2005). Thus, examining the physical causes of the recent summer heatwaves over Europe has important implications for understanding their formation mechanisms, improving their predictability, and for disaster reduction and prevention (Van Oldenborgh et al., 2022; Witze, 2022).

Many factors have been found to contribute to European summer heatwaves (Black & Sutton, 2007; Black et al., 2004; Fischer et al., 2007; Ionita et al., 2020; Li et al., 2020; Schaer et al., 2004; Stott et al., 2004; Vautard et al., 2007; Wang & Luo, 2020; Zhang et al., 2020). Persistent high pressure systems are crucial for the outbreak of summer heatwaves via the continued advection of warm air on the western side of the system and increased surface heating associated with subsidence and increased solar radiation due to reduced cloudiness (Black et al., 2004; Trigo et al., 2005). For example, western European heatwaves can be caused by European blocking (EB)—a persistent high pressure system over central-northern Europe (Stefanon et al., 2012; Trigo et al., 2005), persistent Atlantic ridging and double jet events over Eurasia (Rousi et al., 2021, 2022), teleconnection wave-train patterns (Stefanon et al., 2012), and Ural blocking (UB) (Wang & Luo, 2020). The occurrence region of summer heatwaves over Europe depends on whether EB or UB events take place (Li et al., 2020; Trigo et al., 2005; Wang & Luo, 2020). It is also found that the onset and variability of EB and UB events are mostly linked to the positive phase of North Atlantic Oscillation (NAO) and the variability of the North Atlantic jet on interannual-to-decadal timescales via the propagation of wave trains from the North Atlantic to Eurasia (Luo et al., 2015, 2018). Thus, it is helpful to classify EB and UB events based on the different phase of NAO in order to establish a linkage of UB and EB events to the North Atlantic jet variability, because the European heatwaves depend on EB or UB events and the phase of NAO (Li et al., 2020). Other factors may influence European summer heatwaves, which include warming caused by increased greenhouse gases (GHG) (Fischer & Schar, 2010; Li et al., 2020), soil moisture–atmosphere interactions (Schaer et al., 2004), North Atlantic sea surface temperature (SST) anomalies (Black et al., 2004; Duchez et al., 2016; Sutton & Hodson, 2005), shrinking Arctic sea ice and Eurasian snow cover (Zhang et al., 2020), and favorable antecedent conditions (e.g., winter and spring rainfall deficit over Europe) (Ionita et al., 2020; Rousi et al., 2021; Vautard et al., 2007).

On decadal-to-interdecadal timescales, the variability of western European heatwaves is hypothesized to be tied to the Atlantic Multidecadal Oscillation (AMO)—a mode of North Atlantic SST variability with a period of 60–80 years (Della-Marta et al., 2007; Johnson et al., 2018; Sutton & Hodson, 2005), because AMO-associated North Atlantic SST anomalies may influence Europe through exciting quasi-stationary atmospheric wave trains (Ghosh et al., 2019). However, how the internal AMO variability and GHG-induced warming have contributed to the positive European heatwave trend in the recent decades is unclear (Schaer et al., 2004; Stott et al., 2004), although the warm phase of AMO is found to correspond to decreased summer rainfall over western Europe (Sutton & Hodson, 2005). While the recent AMO variability is linked to decadal changes in external forcing (e.g., volcanic and anthropogenic aerosols) (Qin et al., 2020), GHG-induced warming over Europe can be approximately represented by a linear warming trend (Stott, 2003). In fact, the European air temperature is influenced by not only GHGs and AMO, but also many other factors such as decadal changes in anthropogenic and volcanic aerosols, and other decadal variability (Della-Marta et al., 2007; Stott, 2003). However, Johnson et al. (2018) found that the internal AMO variability plays a major role in the air temperature extremes over Europe. For this reason, GHG-induced warming over Europe can be approximately removed through linear detrending, with the nonlinear component mainly resulting from the AMO-like variability. Thus, in the present paper we hypothesize that the European heatwave trend in recent decades is mainly caused by the GHG-induced warming trend and AMO-like variability.

In this study, we assume that the recent European heatwave trend consists of a GHG-induced component and a nonlinear component, which is mainly correlated with observed AMO. Then, we analyze the reanalysis data and observed gridded data during 1950–2021 to reveal the cause of increased summer heatwaves over Europe in recent decades and quantify the different roles of the recent AMO-like variability and GHG-induced warming through their modulation of the EB and UB events. Using this approach, we are able to estimate the different contributions of the change in the phase of the AMO-like variations and GHG-induced warming to the recent European heatwave trend over 1980–2021. We emphasize that the AMO-like multidecadal variations examined here may be partly forced by decadal changes in external forcing such as anthropogenic and volcanic aerosols (Qin et al., 2020), rather than purely generated by internal AMO.

2. Data and Method

2.1. Data

The daily data from June 1950 to July 2021 (1950–2021) used in this paper were obtained from ERA5 reanalysis (Hersbach et al., 2020), which include daily 500 hPa geopotential height (Z500) and surface or 2 m air temperature (SAT). We also analyzed ERA5 daily Z500 and SAT over western Europe from 11 July to 21 July 2022. The monthly SST data were obtained from the Hadley Center HadISST (Rayner et al., 2003). The daily gridded land-only observational data set for SAT over Europe from the European Climate Assessment and Data set (E-OBS) from 1950 to 2021 derived from in-situ observations was also used at (Cornes et al., 2018; Li et al., 2020). The raw monthly AMO index for summer (June to August, JJA) was taken from this paper are available at (Enfield et al., 2001), which was defined as the area weighted average of the SST anomaly over the North Atlantic (0°N–70°N). The JJA SAT for 25 Phase Six of the Coupled Model Intercomparison Project (CMIP6) models were employed at (Eyring et al., 2016) (Table S1 in Supporting Information S1).

For our composite analysis we use the ERA5 reanalysis SAT data and E-OBS gridded SAT data. While the ERA5 data assimilated surface observations of air temperature, we still use the E-OBS SAT data to validate our results obtained from the ERA5 SAT data. When the detrended data is used, the data set during 1950–2021 is the linearly detrended data at each grid point. Here, the linear trend over 1950–2021 crudely represents the GHG-induced warming trend (Stott, 2003).

2.2. Definition of Heatwaves

In this study, we use summer (JJA) daily-mean SAT anomalies lying above the 90th percentile of their distribution during 1950–2021 to define a heatwave event over Europe and require such SAT anomalies at each grid point to persist for at least three consecutive days and cover a region with at least a 4° lat. × 4° lon. area (Johnson et al., 2018; Rousi et al., 2022). The sum of all heatwave days in a summer is defined as the summer heatwave days (which represents the frequency of heatwaves) and the mean SAT averaged over the heatwave days is used as a measure of heatwave intensity.

2.3. Method for Calculating Trends in Summer Heatwave Days During 1980–2021

In this subsection, we assume that the long-term (decadal and longer) variations in the observed JJA anomalies in SAT or heatwave days or heatwave intensity over Europe can be expressed as

$$T_{\text{obs}} \approx T_{\text{GHG}} + T_{\text{decadal}}, \tag{1}$$

where T_{GHG} is the change induced by GHG increases and T_{decadal} represents decadal-multidecadal changes related to AMO and other decadal variations, including externally forced nonlinear changes. In Equation 1, we hypothesize that the decadal trend of the temperature extremes over Eurasia during 1980–2021 is mainly related to the cold-to-warm phase transition of AMO partly because AMO is within a negative-to-positive phase shift period during 1980–2021 and plays a major role in the decadal change in the summer Eurasian temperatures (Johnson et al., 2018) via modulating the propagation of quasi-stationary atmospheric wave trains from North Atlantic to Eurasia (Ghosh et al., 2019). Here, Europe is defined to be the region (10°W–60°E and 30°N–70°N).

One can obtain from Equation 1:

$$\frac{\partial T_{\text{obs}}}{\partial t} = S_{\text{obs}} \approx S_{\text{GHG}} + S_{\text{decadal}}, \tag{2}$$

where $S_{\text{obs}} = \frac{\partial T_{\text{obs}}}{\partial t}$ represents the long-term slope or trend of the JJA anomalies, t is the time, $S_{\text{GHG}} = \frac{\partial T_{\text{GHG}}}{\partial t}$ is the GHG-induced warming trend, and $S_{\text{decadal}} = \frac{\partial T_{\text{decadal}}}{\partial t}$ is the trend caused by AMO and other decadal variations. Thus, the observed trends in summer European heatwave days during 1980–2021 can be attributed to the GHG-induced warming trend S_{GHG} and a decadal trend S_{decadal} related to AMO and other decadal variations, as shown in Figure 1.

Although the long-term global warming exhibits a nonlinear increasing trend (Franzke, 2014), the GHG-induced warming shows a nearly linear upward trend over Europe during the 20th century with some decadal fluctuations

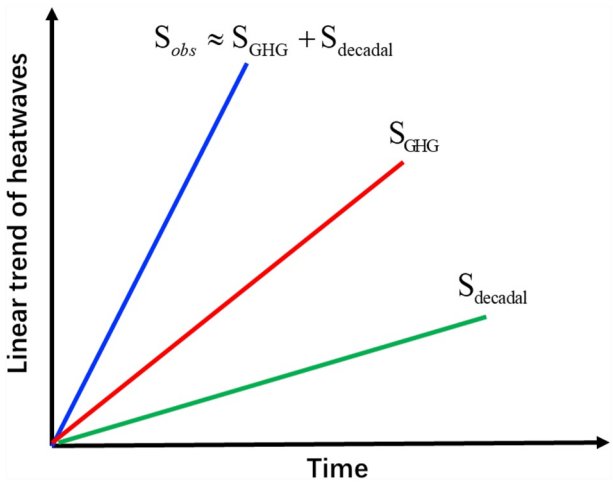

Figure 1. Schematic diagram of the linear trend of European heatwaves consisting of the greenhouse gases (GHG)-induced warming trend S_{GHG} and Atlantic Multidecadal Oscillation (AMO)-related heatwave trend $S_{decadal}$ during 1980–2021.

(Stott, 2003). We estimated S_{GHG} as the linear trend in observed SAT or heatwave days, and $S_{decadal}$ as the decadal trend associated with AMO and other decadal variations. Here, we calculate the trend ratios $R_{GHG} = S_{GHG}/S_{obs}$ and $R_{decadal} = S_{decadal}/S_{obs}$ to reflect the different contributions of GHG-induced warming and AMO and other decadal variations to the observed summer European heatwave changes. To some extent, this approach is able to identify different contributions from the GHG-induced warming and the AMO and decadal variations to observed heatwave changes. In previous studies, the large ensembles of the Coupled Model Intercomparison Project Phase 5 or 6 simulation (CMIP5 or CMIP6) models were used to derive an estimate of the forced SAT response to GHG and other external forcing changes (Dai et al., 2015). However, the obtained forced SAT response still includes some decadal or multidecadal variations (Figures 2a and 2b) because there exist decadal changes in GHGs, volcanic and anthropogenic aerosols, the model uncertainty (Liu et al., 2022) and internal variability (Dai & Bloecker, 2019), which cause nonlinear SAT changes. This suggests that the decadal-multidecadal SAT changes over Europe may be partly forced by externally forcing, rather than purely generated by internal AMO or other climate modes.

Figure 2a shows the time series of the JJA-mean SAT averaged over Europe (10°W–60°E, 30°N–70°N) derived from the ensemble mean of 25 CMIP6 models (Table S1 in Supporting Information S1). It is interesting to note that the CMIP6 model ensemble mean SAT shows a linear increasing trend over 2000–2021 (Figure 2a). Our calculation further shows that the linearly detrended CMIP6 multi-model ensemble-mean JJA SAT anomalies (red line in Figure 2b) have a significant positive correlation of 0.66 ($p < 0.01$) with the linearly detrended JJA AMO index during 1950–2021 (blue line in Figure 2b). For a 9-year low-pass filtered data their correlation coefficient can reach 0.82. This implies that the observed AMO variations are partly forced by decadal variations in external forcing, consistent with previous studies (e.g., Qin et al., 2020). Furthermore, the nonlinear component of the observed JJA SAT over Europe exhibits AMO-like signal variations (Figure 2b). It is further found that the JJA SAT anomaly averaged over Europe detrended by the CMIP6 model ensemble mean has a significant correlation of 0.75 with the linearly detrended domain-averaged SAT anomaly (Figure 2c), indicating that the CMIP6 model ensemble mean detrending does not exhibit a large difference with the linearly detrending. Thus, the CMIP6 model ensemble mean detrending does not significantly remove the decadal change in the Eurasian temperatures. In the following discussions, we also refer to the AMO and externally generated decadal variations as the AMO-like variations. Here we do not attempt to separate the forced and unforced components in the AMO-like variations; instead, we focus on the contributions by the linear warming caused mainly by GHG forcing and the AMO-like (or AMO-related) nonlinear variations, which may result from both external forcing and internal variability.

Because the summer heatwaves in mid-high latitudes are mainly produced by atmospheric blocking with sub-seasonal timescales of 10–20 days, the AMO-related heatwave trend over 1980–2021 is mainly linked to decadal changes in the summer heatwaves modulated by the AMO-like variations via changes in atmospheric blocking events over Eurasia. On the other hand, because the AMO-like variations are slow compared to atmospheric blocking, the phase shift of the AMO-like variations can modulate atmospheric blocking through changing the basic state such as changes in background zonal wind and meridional background potential vorticity gradient (Luo et al., 2019). Thus, to some extent, the phase transition of AMO-like variations and the change in associated North Atlantic jet can be considered as the different background conditions influencing atmospheric blocking.

2.4. Blocking Index

In this paper, our focus is placed on examining the physical cause of the recent summer heatwave trend over Europe. While the European continent is defined by the region (10°W–60°E, 30°N–70°N), the summer heatwaves in this region can be influenced by EB and UB events. In general, EB events mainly occur in the region (10°W–30°E), whereas UB events mainly take place in the region (40°E–80°E) around 60°E.

Here, we use the one-dimensional blocking index presented by Tibaldi and Molteni (1990, TM) to identify EB and UB events occurring in the regions (10°W–30°E) and (40°E–80°E) respectively. The blocking index is

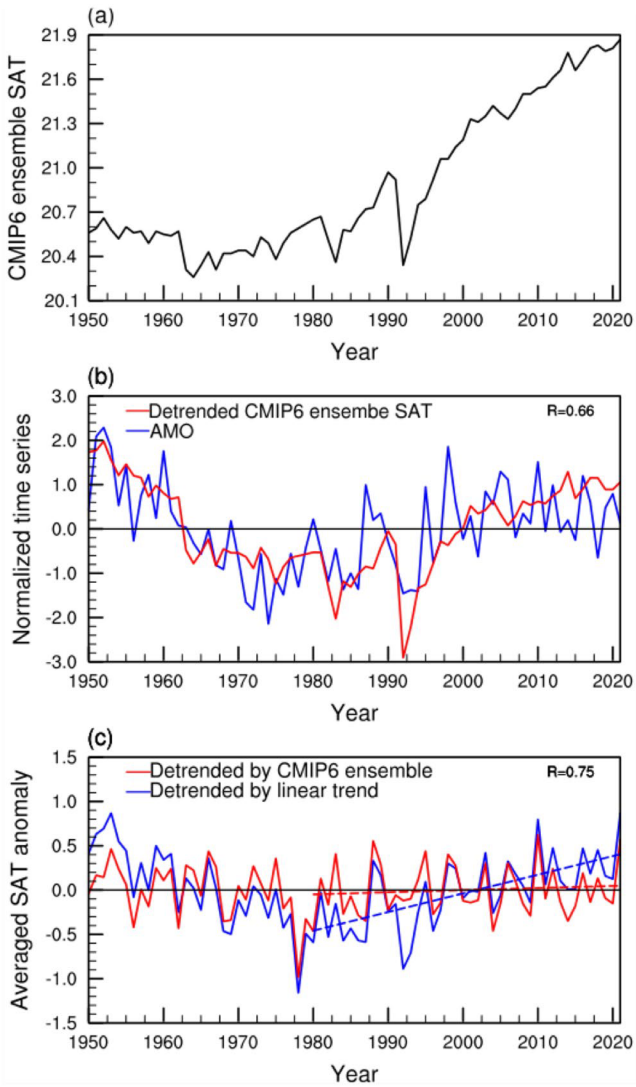

Figure 2. (a) Temporal variation of June, July, and August (JJA) mean surface or 2 m air temperature (SAT) over Europe (10°W–60°E, 30°N–70°N) based on the ensemble mean of 25 Phase Six of the Coupled Model Intercomparison Project (CMIP6) models during 1950–2021. (b) Normalized time series of the linearly detrended CMIP6 model ensemble JJA SAT anomaly averaged over Europe (red line) and Atlantic Multidecadal Oscillation index (blue line) during the 1950–2021 summer. (c) Normalized time series of JJA-mean SAT anomalies averaged over Europe detrended by the CMIP6 model ensemble mean SAT (red line) and linear trend (blue line) respectively. The CMIP6 model ensemble mean is referred to as the CMIP6 ensemble. The value of R denotes the correlation coefficient. In panel (c), the dashed blue line represents the linear trend with the slope rate of 0.2 standard deviations (STDs)/decade of the linearly detrended SAT time series during 1980–2021, whereas the dashed red line denotes the linear trend with the slope rate of 0.02 STDs/decade of the CMIP6 ensemble detrended SAT time series during 1980–2021.

defined based on the reversal of the daily 500-hPa geopotential height (Z500) in mid-to-high latitudes in terms of

$$\mathrm{GHGN} = [\mathrm{Z500}(\phi_N) - \mathrm{Z500}(\phi_o)]/(\phi_N - \phi_o), \quad (3a)$$

$$\mathrm{GHGS} = [\mathrm{Z500}(\phi_o) - \mathrm{Z500}(\phi_S)]/(\phi_o - \phi_S), \quad (3b)$$

at the given three reference latitudes: $\phi_N = 80°\mathrm{N} + \Delta$, $\phi_o = 60°\mathrm{N} + \Delta$, $\phi_S = 40°\mathrm{N} + \Delta$ and $\Delta = -4°, 0°, 4°$ in a fixed longitude. A blocking event is defined to have happened if there are GHGS > 0 and GHGN < −10 gpm (deg lat)$^{-1}$ for at least three consecutive days and for at least one choice of Δ in a given zonal region covering at least 15° of longitude.

2.5. Classification of Blocking Events

Because the frequency, intensity and occurrence region of summer heatwaves over Europe are influenced by EB, UB and the phase of NAO (Li et al., 2020; Wang & Luo, 2020), here we classify EB and UB events according to the phase of NAO. An individual NAO event in summer is defined according to the value of the daily NAO index during the summer (JJA) taken from the NOAA Climate Prediction Center. When the daily NAO index exceeds its mean by at least 0.5 standard deviations (STDs) that persist for at least three consecutive days, a NAO$^+$ (NAO$^-$) event with timescales of 10–20 days can be defined and identified. All other NAO events are defined as neutral NAO (NAO^0) events. The life cycle of the NAO$^+$ (NAO$^-$) event is defined to be a temporal variation that the positive (negative) daily NAO index increases (decreases) to its peak and then decreases (increases) to nearly its beginning value (Luo et al., 2018), where lag 0 is defined to denote the peak day of the NAO$^+$ (NAO$^-$) event, that is, the maximum (minimum) value of the positive (negative) daily NAO index. Because our previous studies have revealed that NAO$^+$ (NAO$^-$) leads (lags) EB or UB by several days (Luo et al., 2015, 2018), in this paper we do not discuss the relationship between EB or UB and the phase of NAO.

Because the value of GHGS is often used to denote the variation of blocking amplitude (Tibaldi & Molteni, 1990), a UB event is considered to be related to the NAO$^+$ (NAO$^-$) event if the peak day of the GHGS associated with UB occurs within the life cycle of the NAO$^+$ (NAO$^-$) event. Here, a UB event with NAO$^+$ (NAO$^-$) is referred to as UB-NAO$^+$ (UB-NAO$^-$) event, whereas a UB event related to neutral NAO is referred to as UB-NAO^0 event (Luo et al., 2017). The EB-NAO$^+$, EB-NAO$^-$, and EB-NAO^0 events can be defined in a similar form.

For each UB (EB) event, its peak day that the blocking amplitude reaches its maximum value can be identified and defined as lag 0. Then we may consider lag 0 as a base point to obtain the evolution field of composite daily Z500 and SAT anomalies for the UB (EB) by performing a daily composite for all UB (EB) events from lag −10 to 10 days. Because the period from lag −5 to 5 days represents the mature phase of the UB (EB), the time-mean fields of composite daily Z500 and SAT anomalies averaged from lag −5 to 5 days can mainly reflect the major role of the UB (EB). The composites of UB-NAO$^+$, UB-NAO$^-$, and UB-NAO^0 or EB-NAO$^+$, EB-NAO$^-$, and EB-NAO^0 events performed are also based on the peak day (lag 0) of each UB or EB event. The composites of individual NAO$^+$ (NAO$^-$) events are based on the peak day (lag 0) of each NAO$^+$ (NAO$^-$) event.

2.6. Statistical Testing

We used a conventional two-sided student's *t*-test to examine the statistical significance in the anomaly field in this paper. The significance of the correlation coefficient and the slope rate of the linear trend is also performed using a conventional student's *t*-test and Mann-Kendall test (Wilks, 2011). Although the conventional *t*-test requires a larger *p* value than that of the False Discovery Rate method (Wilks, 2016), using the two different methods does not change the physical cause of the variability of the SAT anomaly and associated heatwaves. Thus, in this paper, we still use a conventional student *t*-test.

3. Results

3.1. The 2022 Severe Summer European Heatwave and Its Linkage to Ural blocking

Figure 3a shows the time-mean fields of the daily Z500 and its anomaly as well as daily SAT anomalies averaged over the period from 11 to 21 July 2022. It is found that an intense heatwave event occurred in a large region covering the regions 10°W–20°E and 40°E–80°E (Figure 3a) in the 2022 summer, which is accompanied by large positive SAT anomalies over Europe and western Russia that occur together with an atmospheric circulation pattern resembling a combination of UB centered on 60°E with NAO^+ events (Figure 3a). This motivates us to examine the role of UB events with NAO^+ in the summer European heatwaves by performing a composite. According to the time series of summer UB and EB events with different phases of NAO during 1950–2021 (Figure S1 in Supporting Information S1) identified by the TM blocking index, the time-mean fields of composite daily 500-hPa geopotential height (Z500) and SAT anomalies averaged from lag −5 to 5 days (lag 0 denotes the peak day of each blocking event) of UB, UB-NAO^+ and EB-NAO^+ events as defined above are shown in Figure 3b–3d. It is found that a large positive SAT anomaly appeared in a widespread region over Europe for UB-NAO^+ events (Figure 3c) and EB-NAO^+ events (Figure 3d). Clearly, this positive SAT anomaly is more intense and covers a wider domain than those of the UB-NAO^- and UB-NAO^0 events (Figure S2 in Supporting Information S1) as well as all the UB events (i.e., the sum of UB-NAO^+, UB-NAO^-, and UB-NAO^0 events) in summer (Figure 3b).

While the time-mean field of composite UB-NAO^+ events (Figure 3c) differs somewhat from that of the 2022 European heatwave event (Figure 3a), it broadly captures the main feature of the atmospheric circulation pattern leading to the deadly 2022 summer European heatwave with a large SAT anomaly of 3–6 K for a time average of 11 days (Figure 3a). Thus, UB events with NAO^+ can lead to severe heatwaves over most Europe including western Europe with a positive SAT anomaly of 1 K (Figure 3c), which are favored by the meteorological conditions over Europe in recent decades (Della-Marta et al., 2007; Ionita et al., 2020; Vautard et al., 2007). In contrast, positive SAT anomalies occur mainly over eastern Europe and western Russia during UB events with NAO^- as a negative SAT anomaly appears over western Europe (Figure S2 in Supporting Information S1). Consequently, the range and severity of European heatwaves in association with UB events depend on the phase of the NAO. Warm anomalies appear over western, central and northern Europe for all the EB events and their different combinations with the phase of NAO (Figure S2 in Supporting Information S1), which enable heatwaves to occur in these regions. The heatwaves are more intense in the case of NAO^+ (Figure 3d) than its combination with other NAO phases (Figures S2e–S2h in Supporting Information S1). Thus, the positive SAT anomalies associated with EB events are mainly located in western, northern and central Europe, while the SAT anomalies during UB events cover a larger region (Figure S2 in Supporting Information S1), especially nearly entire Europe for UB-NAO^+ events (Figure 3c and Figure S2 in Supporting Information S1). To a large extent, the summer UB-NAO^+ event is an optimal circulation pattern for intense and widespread heatwaves to occur over most Europe except for the southern Europe (Figure 3c).

3.2. Different Roles of the Phase of the AMO-Like Variations and GHG-Induced Warming

The first and second empirical orthogonal function (EOF1 and EOF2) modes of the summer heatwave days over the region (10°W–70°E, 30°N–70°N) during 1950–2021 and their principal component (PC1 and PC2) time series are shown in Figure 4a–4d for the raw (non-detrended) data, whereas the linear trend of the European heatwave days over 1980–2021 is shown in Figure 4e. Correspondingly, the linearly detrended results during 1950–2021 are shown in Figure 5. We can see that for the raw data the PC1 time series (Figure 4c) with 32.9% of

10.1029/2023EF003701

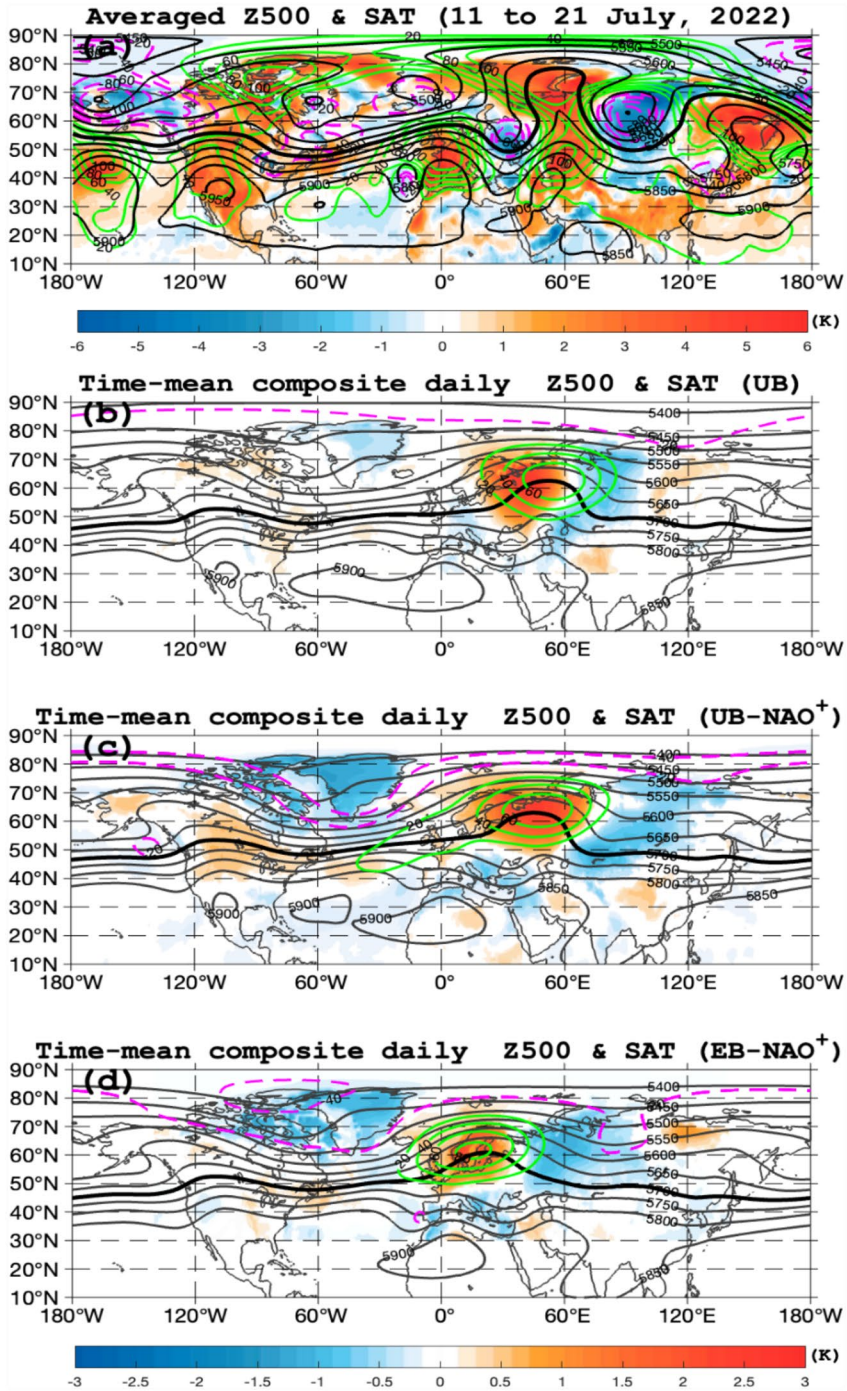

Figure 3. (a) Time-mean daily Z500 (black contours, interval = 50 gpm) field of Ural blocking (UB) event averaged over the period from 11 to 21 July 2022. (b–d) Time-mean composite daily Z500 (green contours, interval = 20 gpm) and surface or 2 m air temperature (SAT) anomalies (color shading, K) averaged from lag-5 to 5 days of (b) all UB events, (c) UB events with NAO^+ (UB-NAO^+ events) and (d) European blocking (EB) events with NAO^+ (EB-NAO^+ events) during 1950–2021 summers based on the ERA5 data. In panels (b–d), the colored regions have SAT anomalies being statistically significant at the 5% level based on a two-sided Student *t*-test. The black contour denotes the time-mean composite daily Z500 field with a thick black line representing 5,700 gpm. Green solid (pink dashed) lines represent positive (negative) Z500 anomalies.

the variance characterizes the temporal variation of the summer heatwaves over the whole Europe for the EOF1 pattern (Figure 4a), which shows an increase in summer European heatwaves over 1998–2021 but a decrease over 1950–1997 (Figure 4c). Clearly, the summer European heatwaves exhibited an increasing trend from 1980 to 2021 (Figure 4e). Because the AMO-like variations show a positive phase mainly during 1998–2021 and

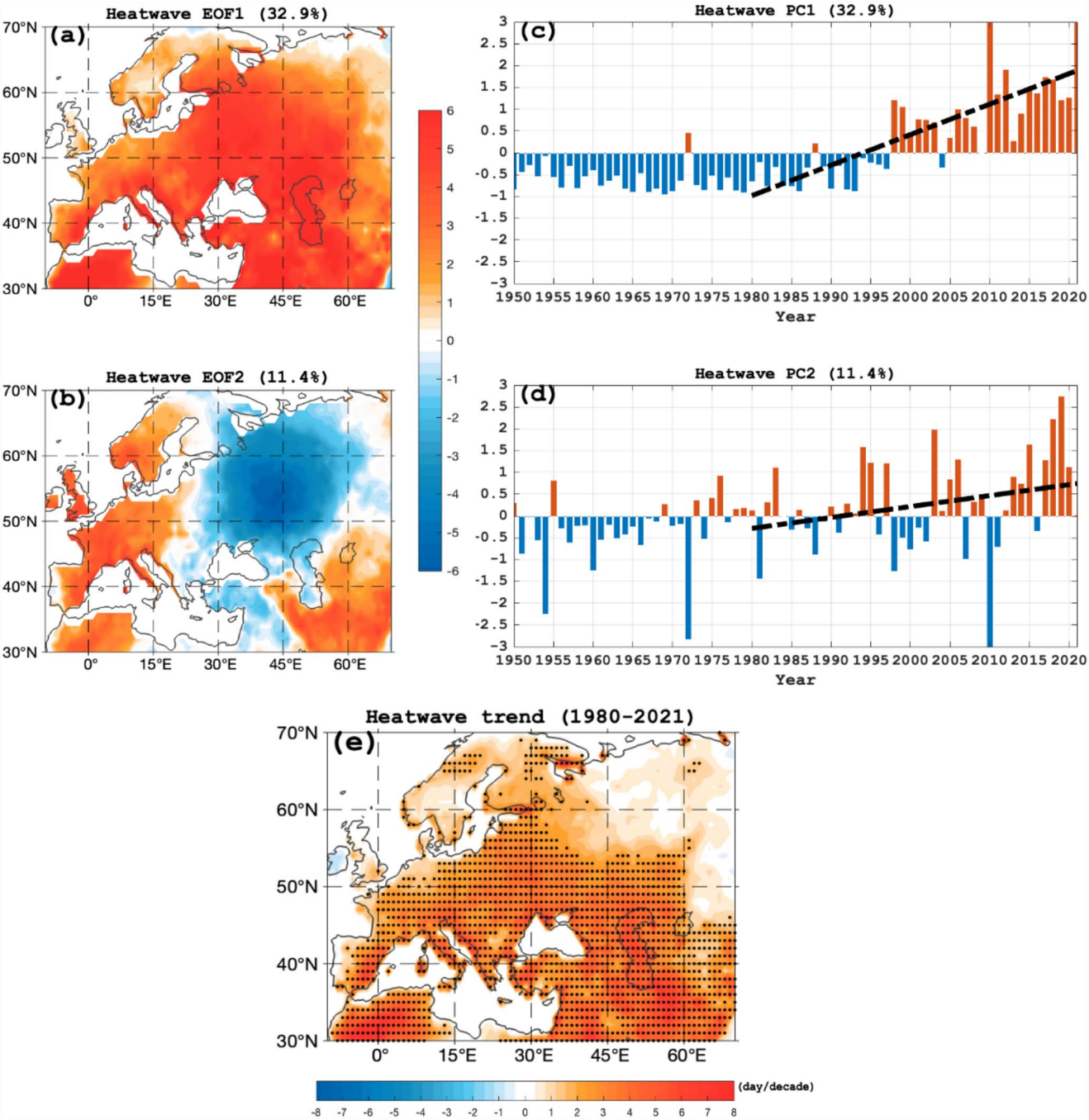

Figure 4. The (a) first and (b) second empirical orthogonal functions (EOF1 and EOF2) of the number of summer heatwave days over Europe (30°N–70°N, 10°W–70°E) during 1950–2021 and (c, d) their normalized (c) PC1 and (d) PC2 time series (PC, bars) based on raw (non-detrended) ERA5 data. (e) Linear trend map of summer heatwave days during 1980–2021 for non-detrended data, where the dot represents the region being significant at the 95% confidence level based on a two-sided student *t*-test. In panels (c–d), the black dashed lines represent linear trends of 0.69 standard deviations (STDs)/decade ($p < 0.01$) and 0.25 STDs/decade ($p < 0.05$) over 1980–2021 of the PC1 and PC2 time series, respectively.

a negative phase mainly during 1962–1997 (Figure 2b), it is inferred that the European heatwave trend over 1980–2021 is not only related to GHG-induced warming, but also related to the shift of the AMO-like variations from the negative to positive phase. The PC2 time series (Figure 4d) with 11.4% of the variance reflects the east-west seesaw of European heatwaves between the western and eastern parts of Europe for the EOF2 pattern

10.1029/2023EF003701

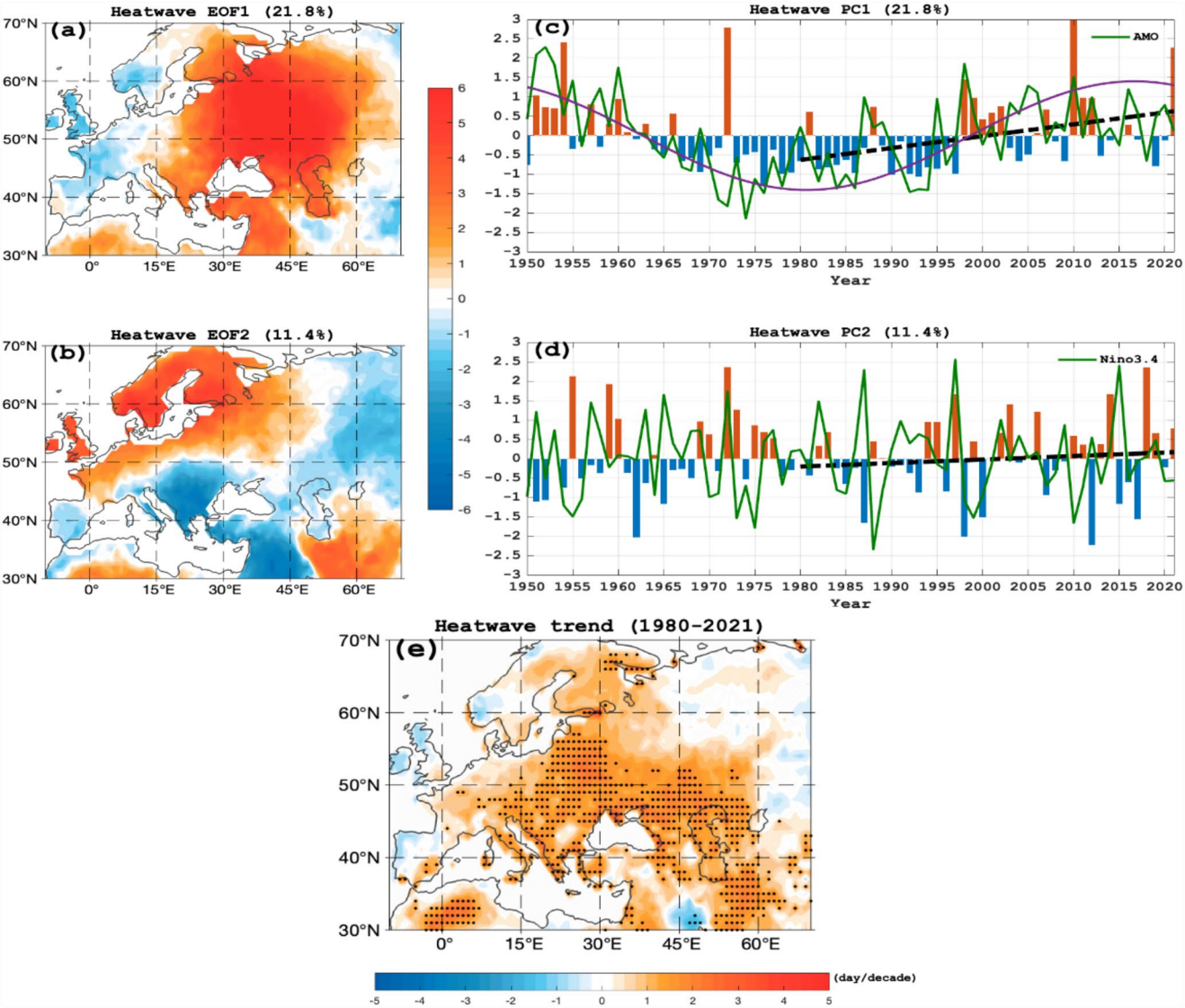

Figure 5. The (a) first and (b) second empirical orthogonal functions (EOF1 and EOF2) of the number of summer heatwave days over Europe (30°N–70°N, 10°W–70°E) during 1950–2021 and (c, d) their normalized (c) PC1 and (d) PC2 time series (PC, bars) based on detrended ERA5 data. (e) Linear trend map of summer heatwave days during 1980–2021 for detrended data, where the dot represents the region being significant at the 95% confidence level based on a two-sided student *t*-test. In panel (c), the black dashed line represents a linear positive trend of 0.3 standard deviations (STDs)/decade ($p < 0.05$) over 1980–2021 in the PC1 time series with the raw summer Atlantic Multidecadal Oscillation index (green line) that is significant at the 99% confidence level and the pink line denotes a 40-year low-pass filtered curve. In panel d, the PC2 time series with the summer Nino3.4 index (green line) has a positive trend of 0.09 STDs/decade ($p > 0.1$) over 1980–2021 (black dashed line).

(Figure 4b). The summer heatwave PC2 time series also exhibits an increasing trend from 1980 to 2021 over northern, western and southern Europe (Figure 4d).

We further find from the linearly detrended data during 1950–2021 (Figure 5) that the PC1, which explains 21.8% of the variance, shows notable interdecadal variations with more heatwave days mainly over central-Eastern Europe (Figure 5a) during 1950–1963 and 1998–2021 and fewer heatwave days during 1964–1997 (Figure 5c). Here, the central-eastern Europe is an extended region that includes central Europe, eastern Europe and western Russia. Calculation reveals that the PC1 time series exhibits an upward trend of 0.3 STDs/decade ($p < 0.05$) from 1980 to 2021 (Figure 5c), but there is a positive slope rate of 0.69 STDs/decade ($p < 0.01$) for its non-detrended data (Figure 4c). Because the non-detrended PC1 (Figure 4c) includes the combined role of the GHG-induced warming and AMO-like variations as well as because the detrended PC1 (Figure 5c) reflects the effect of the AMO-like variations, we can deduce the different contributions of GHG-induced warming and AMO-like

variations to European heatwaves by calculating the ratios of these trends (Figure 1) as described in Section 2. It is not difficult to estimate that approximately 43% of the increased trend of European heatwaves over 1980–2021 comes from the change in the phase of the AMO-like variations, while about 57% of the recent trend results from GHG-induced warming.

The contributions of GHG-induced warming and AMO-like variations can also be estimated by comparing the linear trends of heatwaves over 1980–2021 in Figures 4e and 5e. For example, it is found that the upward trend of heatwave days over the southern part of Europe and central-eastern Europe is estimated to be nearly 3 days/decade for the detrended data (Figure 5e), but about 7 days/decade for the raw (or non-detrended) data (Figure 4e). Obviously, the GHG-induced warming can significantly enhance the recent upward trend of European heatwaves (Stott 2003), particularly in the southern part of Europe and central-eastern Europe (Figures 4a, 4e, 5a, and 5e). When the GHG-induced warming trend is removed for the heatwave PC1 time series (Figure 5c), the upward trend of heatwaves cannot be seen over the western Europe and northern Europe (Figure 5a). But significant trends can still be seen over central, eastern Europe and western Russia (Figure 5e), while they are weaker than those of non-detrended results (Figure 4e). Thus, the recent increasing heatwave trend over central, eastern Europe and western Russia is mainly due to the combined effect of the AMO-like variations and GHG-induced warming. The EOF2 (Figures 5b and 5d) represents an interannual mode, likely linked to the modulation of El Nino–Southern Oscillation (ENSO) (Schneidereit et al., 2012) and North Atlantic SST tripole (Li et al., 2020; Mecking et al., 2019). This EOF2 mode (Figure 4b) with its positive PC2 value (Figure 4d) has more heatwave days over western, northern Europe and the part of southern Europe for non-detrended data and exhibits a linear upward trend over 1980–2021 (Figure 4d). However, it has more heatwave days over western, northern Europe and the part of western Russia (Figures 5b and 5d), and no significant upward trends over 1980–2021 for a linearly detrended data (Figure 5d). Thus, the significant upward trends of heatwave days over western and northern Europe over 1980–2021 (Rousi et al., 2022) are mainly due to GHG-induced warming.

3.3. Role of the North Atlantic Jet Variability Mediated by the Phase of the AMO-Like Variations

Although a sub-seasonal UB-NAO$^+$ event is a key factor for severe and widespread heatwaves over most Europe, its event number does not show notable increases during 1980–2021 for a linearly detrended data from 1950 to 2021 (Figure S1b in Supporting Information S1). Thus, the change in the number of UB-NAO$^+$ events cannot explain the increasing trend in European heatwaves during 1980–2021 (Figures 5c and 5e). However, because NAO events are mainly driven by synoptic-scale eddies and because changes in UB and EB events are related to the phase of NAO and the strength of midlatitude North Atlantic jet (Luo et al., 2015), the multidecadal variability of European heatwaves is likely linked to the change in the phase of AMO-like variations via interdecadal changes in the location, scale, movement and persistence of sub-seasonal UB and EB events due to the interdecadal variability of the North Atlantic jet. Although Rousi et al. (2022) emphasized the role of double jets over Eurasia in Eurasian heatwaves, their double jet events essentially correspond to atmospheric blocking events over Eurasia. The double jet events over Eurasia can reflect the sub-seasonal (10–20 days) variability of zonal winds over Eurasia, but cannot reflect the variability of North Atlantic jet modulated by the shift of the AMO-like variations from the negative to positive phase.

Because NAO, EB, and UB events are of subseasonal timescales (10–20 days), we can use a 30-days filter to remove individual NAO, EB, and UB events to obtain the basic atmospheric state with timescales longer than those of NAO, EB, and UB events. The change in the basic atmospheric state can be considered as different background conditions influencing NAO and atmospheric blocking (Luo et al., 2018, 2019). As a result, it is inferred that the variability of the North Atlantic jet modulated by the phase of the AMO-like variations can significantly influence NAO, EB, and UB events (Luo et al., 2015, 2018). We used 30-days low-pass filtered daily 500-hPa zonal wind (U500) fields based on the detrended ERA5 reanalysis data to calculate the EOF1 mode of the JJA-mean North Atlantic zonal winds over the North Atlantic to obtain the variability of the North Atlantic jet in strength and location on interannual-to-interdecadal timescales. The EOF1 of JJA-mean U500 over the North Atlantic (80°W–0°W, 20°N–70°N) and its corresponding PC1 time series are shown in Figures 6a and 6b. It is seen that the U500 EOF1 mode, which explains 37% of the variance and multidecadal variations similar to those of the heatwaves (Figure 5c; $r = 0.67$ for 9-year smoothed data and $r = 0.99$ for 40-year smoothed data), reflects multidecdal changes in the strength of the North Atlantic jet represented by the red contours of the climatological zonal wind exceeding 5 m/s in Figure 6a. This mode suggests a strong (weak) jet over the North Atlantic midlatitudes (30°N–50°N) during 1950–1963 and 1998–2021 (1964–1997), with the jet extending toward European high latitudes (Figure 6a), even though its intensity shows an upward trend of 0.18 STDs/decade ($p < 0.05$) over

10.1029/2023EF003701

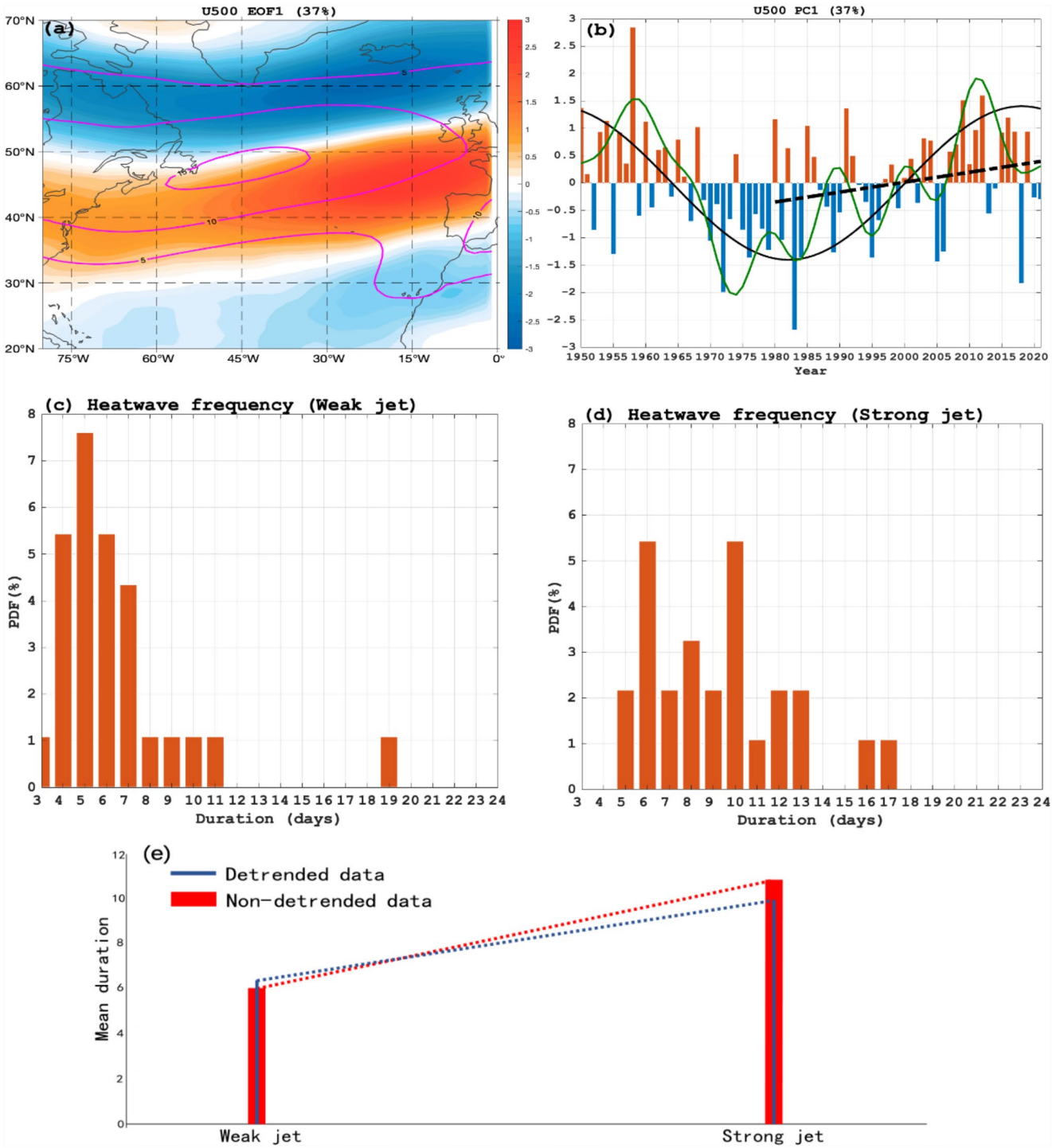

Figure 6. (a) The first empirical orthogonal function (EOF1) of June, July, and August (JJA)-mean 30-days low pass filtered U500 anomaly over North Atlantic (20°N–70°N, 80°W–0°W) and (b) normalized time series of its corresponding principal component (PC1, bars) during the 1950–2021 summers for detrended data. In panel (b), the black dashed line represents a linear trend with a slope rate of 0.18 standard deviations (STDs)/decade ($p < 0.05$) over 1980–2021 and the green (black) line denotes a 9-year (40-year) low-pass filtered curve. (c, d) Probability distribution function (PDF) of the heatwave frequency (days) averaged over the region (20°E–55°E, 40°N–55°N) with the duration of the heatwave event during 1950–2021 for (c) weak and (d) strong midlatitude North Atlantic jet summers. In panels (c–e), the value of 40-year low pass filtered summer U500 PC1 time series having at least −0.5 (0.5) STDs is defined as a weak (strong) midlatitude North Atlantic jet or a weak (strong) jet. (e) Linear trend of the mean duration of European heatwaves between weak and strong jets for detrended (dashed blue line) and non-detrended (dashed red line) data.

1980–2021 (Figure 6b). These results suggest that the increased European heatwaves from 1980 to 2021 are linked to the interdecadal intensification of the midlatitude North Atlantic jet.

If the value of the detrended 40-year low pass filtered JJA-mean U500 PC1 time series with ≥0.5 (≤−0.5) STDs is defined as a strong (weak) North Atlantic jet or PC1$^+$ (PC1$^-$) in the North Atlantic, then there are 27 weak and 27 strong jet summers during 1950–2021. The strong (weak) North Atlantic jet is sometimes referred to as the strong (weak) jet hereafter. It can be seen that the summer heatwaves are longer lasting over the region (20°E–55°E, 40°N–55°N) for a strong jet (Figure 6d) than for a weak jet (Figure 6c). The mean duration of the heatwave events in the region is 6.4 days for a weak jet, but 9.9 days for a strong jet (Figure 6), while they are 6 and 10.8 days respectively for a raw (non-detrended) data (Figure S3 in Supporting Information S1). Clearly, the intensification of the midlatitude North Atlantic jet can cause a significant increase in the mean duration of heatwaves over Europe and western Russia, whereas GHG-induced warming favors an increase (decrease) in the mean duration of European heatwaves under a strong (weak) jet. In particular, the GHG-induced warming can significantly increase the difference of the mean heatwave duration between strong and weak jets. Thus, whether GHG-induced warming favors the persistent European heatwaves depends on if the North Atlantic jet is strong. From these numbers it is estimated that the increase in the linear upward trend of the mean duration of European heatwaves from a weak to strong jet is 37% due to GHG-induced warming (Figure 6e). Thus, GHG-induced warming can significantly amplify the upward trend of recent heatwaves associated with intensified North Atlantic jet. Composites of the UB-NAO$^+$ events are shown in Figure 7 for strong and weak North Atlantic jet cases. We find that the anticyclonic center of the UB-NAO$^+$ is located in the Ural Mountains near 70°N under a weak jet (Figure 7a), but near 60°N under a strong jet (Figure 7b). The warm anomaly during UB-NAO$^+$ events is more persistent and intense over central-eastern Europe under a strong jet (Figure 7b) than under a weak jet (Figure 7a). This is because the UB with NAO$^+$ shows lesser movement, longer lifetime, slower decay and larger zonal width due to smaller meridional potential vorticity gradient over Eurasia (Luo et al., 2019) under a strong North Atlantic jet (Figure 7h) than under a weak North Atlantic jet (Figure 7g) and thus is accompanied by longer-lasting dry surface, lower clouds and stronger surface solar heating under a strong jet. The UB is also accompanied by a stronger cyclonic anomaly over central Eurasia (the east of 60°E) which affects the Z500 and SAT anomalies over eastern Europe and western Russia under a weak jet (Figure 7a), while the cyclonic anomaly is weak or absent under a strong jet (Figure 7b). Given this spatial difference in the SAT anomalies (Figure 7c), the recent intensification of the midlatitude North Atlantic jet (Figures 6a and 6b) contributes to the increased heatwave days over Europe during 1980–2021 (Figure 5e). In our results, the difference of the SAT anomaly associated with UB-NAO$^+$ events between strong and weak jets (Figure 7c) can explain why the linear upward trend of European heatwaves over 1980–2021 mainly occurs in the latitude region 40°N–60°N (Figure 5e). Moreover, the detrended ERA5 results are consistent with those of the detrended E-OBS daily gridded data (Figures 7d–7f), although the E-OBS data do not cover the region east of 45°E. Similar results are also found for UB-NAO$^+$ events based on a 9-year low pass filtered detrended U500 PC1 time series (Figure S4 in Supporting Information S1).

Because negative SAT anomalies appear over western and northern Europe for the UB with NAO$^-$ (Figure S2c in Supporting Information S1), warm anomalies appear mainly over central-eastern Europe for a composite of all UB events (Figure S5 in Supporting Information S1). The enhancement of the UB-induced warm anomaly from a weak to strong jet occurs mainly over central-eastern Europe (Figures S5c and S5f in Supporting Information S1, strong minus weak fields). We further see that the composite of all the EB events (i.e., the sum of EB-NAO$^+$, EB-NAO$^-$, and EB-NAO^0 events) show warm anomalies over western, central and northern Europe because the EB event is accompanied by increased solar heating, reduced clouds and precipitation in these regions (Trigo et al., 2005). This EB-induced warm anomaly is also influenced by the intensity of the midlatitude North Atlantic jet. A large increase in the warm anomaly between two jet states appears over most Europe except very eastern part of Europe because the EB has stronger anticyclonic anomaly over the high latitudes (50°N–70°N) to the east and south of Scandinavia under a strong jet than under a weak jet (Figure S6 in Supporting Information S1). It is noted that the Z500 and SAT of the UB-NAO$^+$ or all UB and EB events do not show a positive anomaly change over northern Europe from a weak to strong jet (Figure 7c and Figures S5 and S6 in Supporting Information S1), thus explaining the weak trend of heatwaves there (Figure 5e). We also see that the heatwaves are longer lasting over central-eastern Europe under a strong jet (Figures 6c and 6d) because the UB and EB have larger zonal scale, longer persistence, slower decay and lesser zonal movement under a strong jet than under a weak jet (Figure S7 in Supporting Information S1), even though EB events are more frequent than UB events (Figure S1 in Supporting Information S1). Since 1998–2021 (1980–1997) corresponds to a strong (weak) North Atlantic jet in the

10.1029/2023EF003701

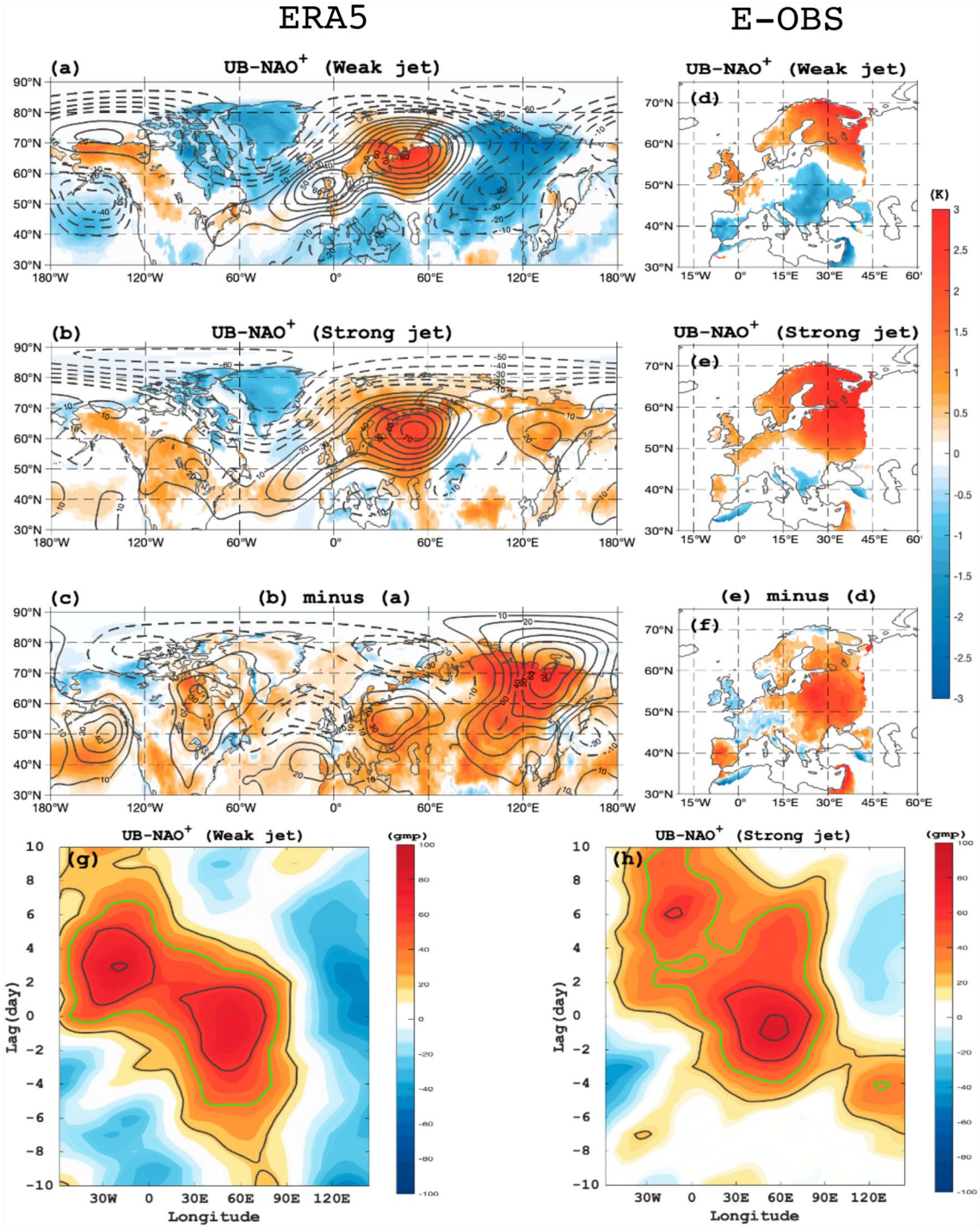

Figure 7. (a–f) Time-mean composite daily Z500 (contours) and surface or 2 m air temperature (SAT) (color shading) anomalies averaged from lag −5 to 5 days of UB-NAO$^+$ events during (a, d) weak (27 cases) and (b, e) strong (27 cases) North Atlantic jet (weak and strong jet) summers and (c, f) their differences for (a–c) ERA5 and (d–f) E-OBS data based on 40-year low pass filtered U500 principal component (PC1) time series, where lag 0 denotes the peak day of the Ural blocking (UB) event. (g, h) Time-longitude evolution of composite daily Z500 anomalies averaged over (50°N–70°N) of UB-NAO$^+$ events for (g) weak and (h) strong jet summers, where the green contour denotes 40 gpm. The duration of the UB in the Ural region (40°E–80°E) is estimated to be about 8 (10.5 days) by calculating the persistence time of the 40-gpm contour between the beginning and end. In panels (a–f), the color shading indicates that the SAT anomalies are significant at the 95% confidence level based on a two-sided Student *t*-test.

midlatitudes (30°N–50°N), the sub-seasonal SAT anomaly associated with all UB and EB events in summer should show decadal intensification over most Europe from 1980–1997 to 1998–2021, thus contributing to the increasing trend of summer heatwaves over Europe during 1980–2021 (Figure 5e). This leads us to speculate that the recent increased summer heatwave trend over Europe is partly due to the interdecadal intensification of the midlatitude North Atlantic jet.

Because the internal AMO variability has a significant contribution to the observed summer SAT change or air temperature extremes over Europe (Johnson et al., 2018), here we used the linearly detrended JJA AMO index over 1950–2021 to examine the physical mechanism of how the AMO-like variations influence summer European heatwaves through changing North Atlantic jet. The change in the phase of the AMO is believed to cause decadal changes in the North Atlantic jet as suggested previously (Hall et al., 2017) and seen in Figures 6a and 6b. The detrended summer AMO index (Figure 8a) is mostly positive during 1950–1963 and 1998–2021 but mostly negative during 1964–1997, which has an upward trend of 0.31 STDs/decade ($p < 0.05$) over 1980–2021 close to the PC1 heatwave trend in the same time interval (Figure 5c) and is positively correlated with the summer U500 PC1 (Figure 6b) ($r = 0.22$, $p < 0.1$). The correlation increases to 0.80 and 0.99 for the 9-year and 40-year low pass filtered data. Thus, in the absence of GHG-induced warming the European heatwave trend over 1980–2021 is mainly determined by the variation of the recent AMO index via changes in the midlatitude North Atlantic jet. The regressed summer SST, Z500, and U500 anomalies onto the detrended 40-year low-pass filtered AMO index (Figures 8b–8d) show that for a positive AMO index the warm SST anomalies are mainly located in the Gulf Stream extension and its southeast side, but relatively weak in the mid-to-high latitude region of North Atlantic near the coasts of UK and Norway. Such warm SST distributions (Figure 8b) are associated with intensified midlatitude North Atlantic zonal winds mainly in the east of 40°W and in the latitudes 37°N–54°N which further extend to the high latitudes of Eurasia (Figure 8d). The enhancement of the midlatitude North Atlantic jet is due to the presence of a stationary cyclonic anomaly in the east of North Atlantic (46°N–62°N) (Figure 8c) associated with a negative-phase summer NAO-like pattern on interdecadal timescale (O'Reilly et al., 2017). The opposite is seen for a negative AMO phase. Thus, a warm (cold) AMO phase favors a strong (weak) midlatitude North Atlantic jet. For a cold AMO, reduced zonal winds are seen in the Eurasian high latitudes to the north of about 60°N (an opposite pattern of Figure 8d), which favors the occurrence of high-latitude UB (Figure 7a). In contrast, the low-latitude UB (Figure 7b) is favored by a warm AMO due to reduced zonal winds over Eurasian midlatitudes to the south of about 60°N (Figure 8d). Thus, a warm (cold) AMO phase tends to favor (suppress) European hot days through producing low-latitude (high-latitude) UB events with long (short) lifetime, large (small) zonal width, slow (rapid) decay and weak (strong) retrogression (Figures 7g–7h and Figure S7 in Supporting Information S1) via the intensified (weakened) midlatitude North Atlantic jet and its extension to the Eurasian continent. Such a relationship is evident because the detrended heatwave PC1 time series has positive correlations of 0.39 ($p < 0.05$), 0.73 and 0.99 with the detrended summer AMO index for the unfiltered, 9-year and 40-year low-pass filtered data. We also note that the composite results of UB and EB events for the warm (cold) AMO phase (Figures S8–S11 in Supporting Information S1) resemble those for strong (weak) jet (Figures S5 and S6 in Supporting Information S1) because the detrended AMO index has a positive correlation of 0.80 (0.99) with the detrended U500 PC1 series for a 9-year (40-year) low-pass filtered data.

3.4. Differing Contributions of Ural Blocking and European Blocking to European Heatwaves

While the summer NAO events frequently occur in the North Atlantic (Figure S13 in Supporting Information S1) and have significant sub-seasonal timescales, the summer NAO-like patterns also possess interannual and interdecadal variabilities (Ghosh et al., 2019; O'Reilly et al., 2017) which are modulated by variabilities in ENSO and AMO (Folland et al., 2009). The interdecadal NAO-like pattern and associated North Atlantic jet as background conditions can influence sub-seasonal NAO events and associated downstream blocking (EB and UB) events (Luo et al., 2015). This is because the NAO^- events mainly result from the retrogression of amplified ridges over northern Europe or Ural region (Yao & Luo, 2015) and the EB or UB events stem from the energy dispersion of Rossby waves due to decay of NAO^+ (Luo et al., 2018). This motivates us to examine whether the NAO events and the total effect of EB and UB events lead to enhanced warm anomalies over Europe from a cold AMO to warm phase to explain the increased trend of summer European heatwaves over 1980–2021. Similar to the above jet strength definition, we also define the value of 40-year low-pass filtered summer AMO index with ≥ 0.5 (≤ -0.5) STDs as a warm (cold) AMO phase or AMO^+ (AMO^-). Composites of EB plus UB (EB + UB) events show that warm anomalies associated with the total effect of EB and UB events mainly appear over western and

10.1029/2023EF003701

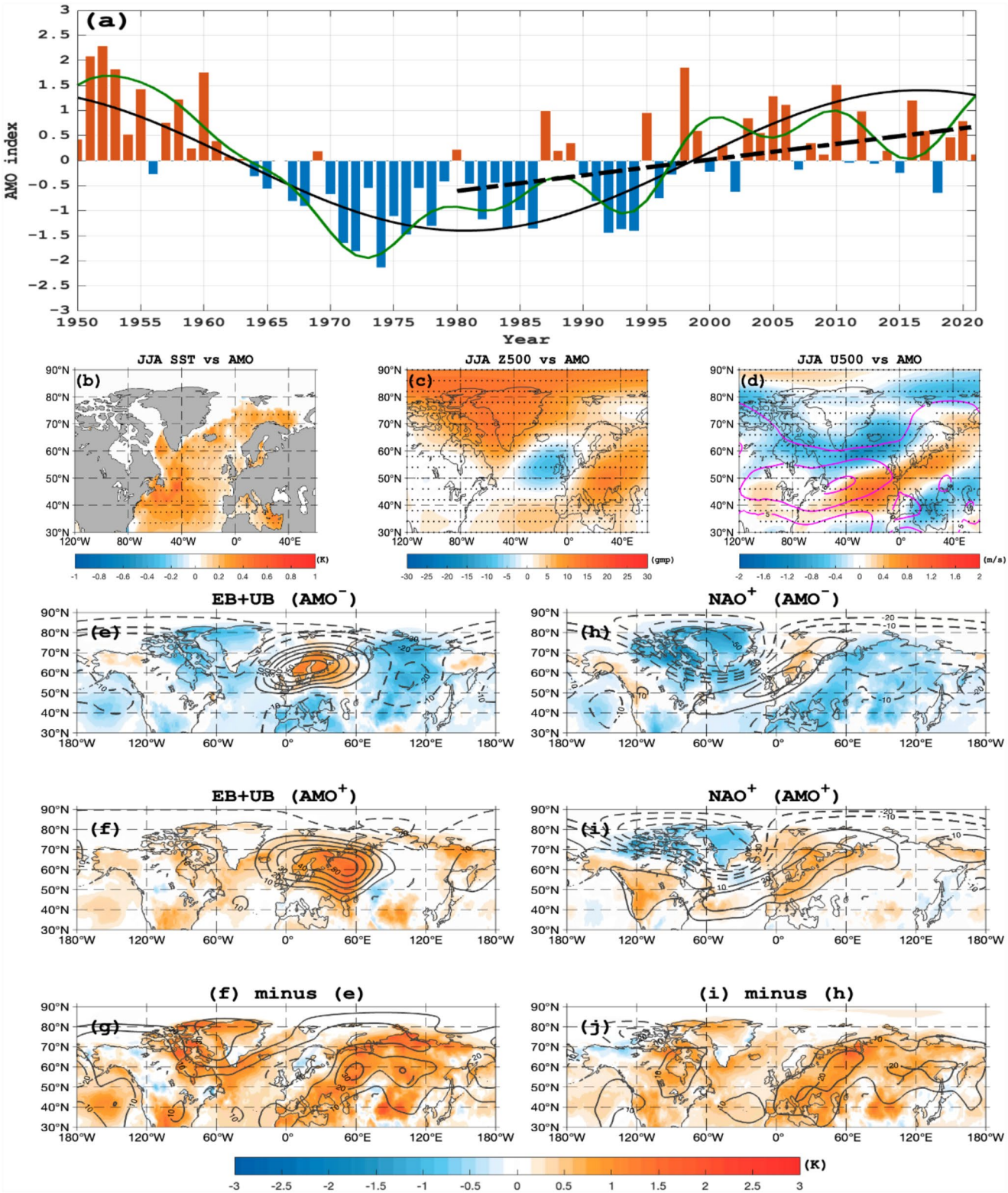

Figure 8.

northern Europe for a cold AMO phase (Figure 8e), but over most Europe and western Russia for a warm AMO phase (Figure 8f). We also see that the EB + UB pattern exhibits an UB for a warm AMO phase (Figure 8f), whereas it more resembles an EB for a cold AMO phase (Figure 8e). Considering the total effect of EB and UB events, an enhanced warm anomaly is seen over central, eastern and southern Europe as the AMO experiences a shift from a cold to warm phase (Figure 8g).

For a cold AMO phase the anticyclonic anomaly of the NAO^+ undergoes an eastward extension from UK to Baltic Sea and Scandinavia along the southwest-northeast direction (Figure 8h) based on composites of NAO^+ events for their time series (Figures S12 and S13 in Supporting Information S1). This NAO^+ leads to weak warm anomalies over western and northern Europe (Figure 8h). However, for a warm AMO phase the NAO^+ can produce widespread anticyclonic and thus warm anomalies over most Europe and the Arctic regions near Ural Mountains and the Barents-Kara Seas. Such a widespread anticyclonic anomaly is attributed to an enhanced energy dispersion of the NAO^+ associated with a strengthened midlatitude North Atlantic jet due to intensified meridional potential vorticity gradient in the North Atlantic (Luo et al., 2018). Thus, the NAO^+ can lead to more intense and widespread anticyclonic anomalies over Europe under AMO^+ (Figure 8i) than under AMO^- (Figure 8h). The intensification of the NAO^+-induced warm anomaly from the AMO^- to AMO^+ is also evident over most Europe (Figure 8j). However, a strong warm anomaly associated with the NAO^- under the warm AMO phase appears only in southeastern Europe (Figure S14 in Supporting Information S1). Of note is that the NAO^+ (NAO^-) without concurrent blocking (UB and EB) (Figures S13 and S15 in Supporting Information S1) cannot produce strong warm anomalies over most Europe besides weak warm anomalies over southern Europe and the Mediterranean Sea, presumably due to the eastward extension of the NAO^+ anticyclonic anomaly (the generation of a weak anticyclonic anomaly due to wave train propagation related to the NAO^-) (Figure S15 in Supporting Information S1). This indicates that the EB and UB events still play a major role in the occurrence of summer hot days over Europe associated with NAO^+ and NAO^- events, even though the effects of NAO^+ and NAO^- events depend strongly on the phase of the AMO. For a warm AMO phase, the NAO^+ (NAO^-) mainly influences SAT over high-latitude (low-latitude) Europe (Figure 8 and Figure S14 in Supporting Information S1). We also find that the impact of the AMO's phase through EB, UB, NAO^+, and NAO^- events on SAT is weak over western and northern Europe (Figures 7 and 8 and Figure S14 in Supporting Information S1), indicating that the transition of the AMO's phase cannot produce a significant heatwave trend over western and northern Europe in the absence of GHG-induced warming. Using the time-mean SAT anomalies averaged over the blocking life period from lag −10 to 10 days of EB and UB events, one can obtain the normalized EB- and UB-related summer SAT time series (Figures 9a and 9b). By comparing their linear trends over 1980–2021, it is easily estimated that the EB (UB) can contribute to nearly 55% (42%) of the AMO-related heatwave trend over central-eastern Europe (20°E–55°E, 40°N–55°N) from 1980 to 2021 according to the reconstructed summer SAT time series based on a linear regression (Figure 9c).

4. Conclusions and Discussion

In this paper we found that the increasing trend in summer European heat waves over central, eastern, southern Europe and western Russia since 1980 is closely related to the interdecadal change in the summer-mean effects of EB and UB events or the UB and EB events concurrent with NAO^+ events that are modulated by the recent cold-to-warm phase transition of the AMO-like variations that may be partly forced by external forcing. Our results provide new evidence that while the European heatwaves are produced by EB or UB occurrences (Li et al., 2020; Stefanon et al., 2012; Trigo et al., 2005; Wang & Luo, 2020), their area extent and intensity depend strongly on whether the EB or UB is concurrent with the positive phase of NAO and whether the midlatitude North Atlantic jet is strong, which is, in turn, affected by the AMO. Without the role of concurrent UB or EB events, the summer NAO events cannot produce strong European heatwaves (Figure S15 in Supporting Information S1). Thus, EB or UB is a key ingredient for the generation of

Figure 8. (a) Time series of normalized summer Atlantic Multidecadal Oscillation (AMO) index (bars) with a linear trend of 0.31 standard deviation/decade ($p < 0.05$) over 1980–2021 (black dashed line) and 9- (green line) and 40- (black solid line) year low-pass filtered curves. (b–d) Regressed summer (b) sea surface temperature, 30-days low pass filtered (c) Z500 (shading) and (d) U500 (shading) anomalies against the 40-yr low pass filtered summer AMO index. (e–j) Time-mean composite daily Z500 and surface or 2 m air temperature (SAT) anomalies averaged from lag −5 to 5 days of (e–g) European blocking (EB) plus Ural blocking (UB) (EB + UB, lag 0 denotes the peak day of blocking) and (h–j) NAO^+ events (lag 0 represents the peak day of the North Atlantic Oscillation (NAO) and NAO^+ represents the positive phase of NAO) during the (e, h) AMO^- and (f, i) AMO^+ summers and (g, j) their differences. The dot (color shading) in panels (b–d), (e–j) represents the values being significant at the 95% confidence level based on a two-sided student's *t*-test. In panel (d), the pink contour denotes the spatial distribution of summer climatological zonal winds with at least 5 m/s.

10.1029/2023EF003701

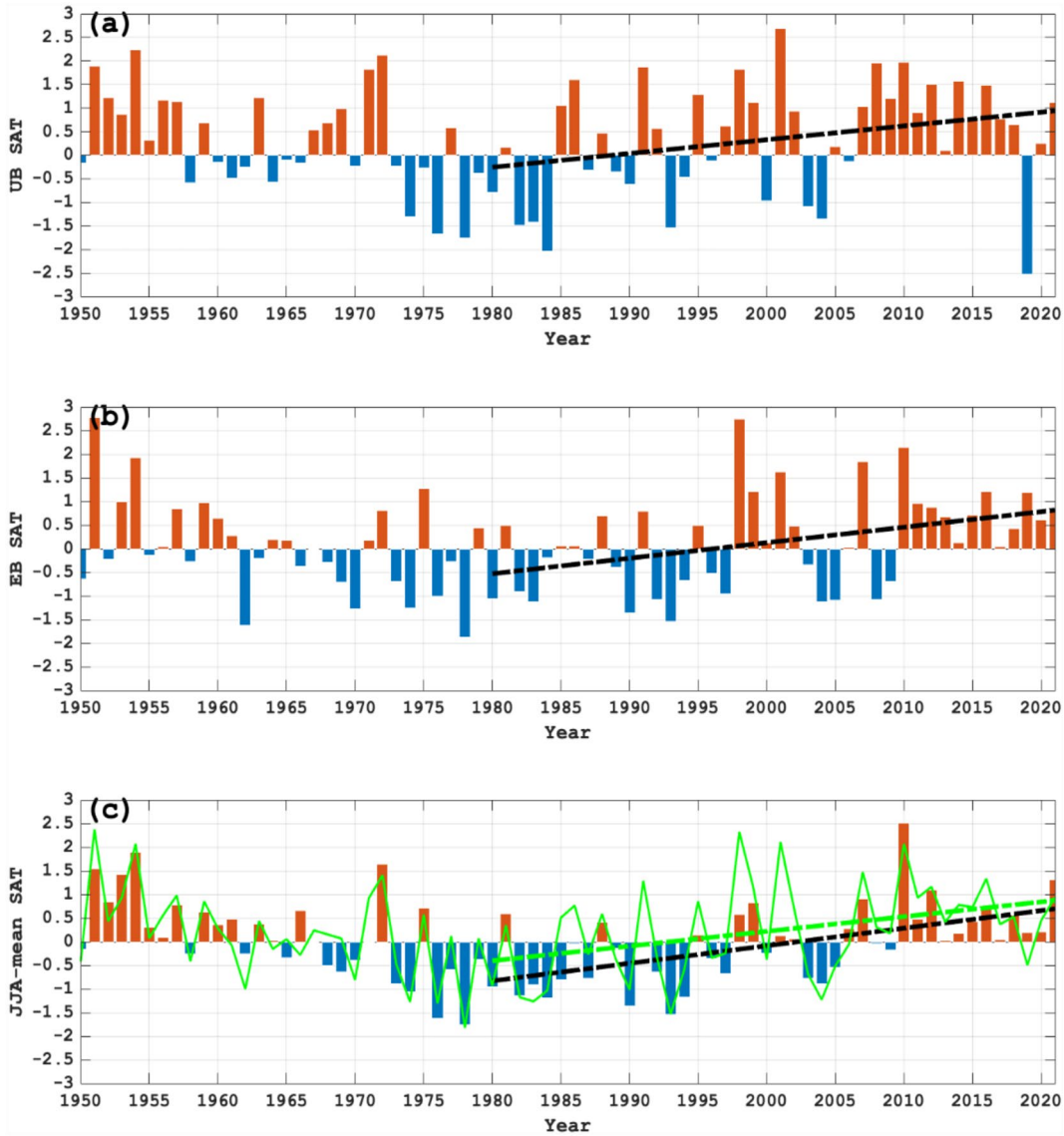

Figure 9. Normalized time series of time-mean composite daily surface or 2 m air temperature (SAT) anomalies averaged from lag −10 to 10 days and over the region (20°E–55°E, 40°N–55°N) for (a) Ural blocking (UB) and (b) European blocking (EB) events. (c) Normalized time series of June, July, and August (JJA)-mean SAT anomalies averaged over the region (bars) with a reconstructed JJA-mean SAT time series (green line) in terms of the UB and EB-induced SAT variations. The black and green dashed lines represent their linear trends over 1980–2021. The reconstructed time series with a 1980–2021 linear trend (green dashed line) has a positive correlation of 0.82 ($p < 0.01$) with the JJA-mean SAT time series.

summer European heatwaves even in the presence of NAO events, while European heatwaves are linked to double jet events over Eurasia and Atlantic ridge (Rousi et al., 2021, 2022). Here, we present new findings that the recent upward trend of heatwaves over western and northern Europe is mainly attributed to GHG-induced warming, whereas the recent heatwave trend over central-eastern Europe (including western Russia) and part of southern Europe is primarily due to the joint role of the recent cold-to-warm transition of the AMO-like variations and GHG-induced warming. In particular, the GHG-induced warming as an amplifier can enhance the recent European heatwave trend induced by the internal variability (i.e., the positive phase of AMO-like variations). However, without the participation of atmospheric blocking events the GHG-induced warming cannot directly produce heatwave events over Europe.

Our estimate also reveals that approximately 43% of the recent heatwave trend over 1980–2021 over central-eastern Europe results from the shift of the AMO's phase from a cold to warm phase (which may be partly forced by external forcing), while about 57% of this heatwave trend is related to GHG-induced warm-

ing. It is further estimated that EB (UB) can make a contribution to about 55% (42%) of the AMO-related heatwave trend over central-eastern Europe in recent decades. In fact, Zhang et al. (2020) noted that the increased trend of recent European heat waves is also related to summer Arctic sea ice loss. Thus, the recent increasing trend in summer heatwaves over Europe is partly caused by the shift of the AMO-like variations from a cold to warm phase through the intensification of the midlatitude North Atlantic jet and its influence on EB and UB events, whereas GHG-induced warming can significantly amplify this increasing trend. To some extent, an intensifying of the midlatitude North Atlantic jet associated with the cold-to-warm phase shift of AMO is a precursor background signal for whether intense and widespread European heatwaves take place over Europe including western Russia. We also find that whether GHG-induced warming significantly influences European heatwave events depends on the strength of the midlatitude North Atlantic jet or the phase of AMO. The GHG-induced warming may play a favored (suppressed) role for European heatwave events when the midlatitude North Atlantic jet is strong (weak) or when AMO is in a warm (cold) phase period.

While CMIP5 models capture the mean heatwave characteristics (Schoetter et al., 2015), they are unable to realistically simulate specific events (e.g., the 2003 heat wave) probably because of the underestimation of atmospheric blocking or different realization of the internal variability. Compared to CMIP5, CMIP6 can simulate stronger warming trend over Europe due to increased GHG (Wyser et al., 2020). Nevertheless, the CMIP6 models seem to still underestimate the occurrence and severity of Northern Hemispheric blocking (Simpson et al., 2020). Under GHG-induced warming, the heat waves become more frequent and have higher mean duration, extent and intensity (Schoetter et al., 2015). This supports our results that more than half of the recent European heatwave trend is attributed to increased GHGs. However, our results further reveal that the positive phase of the AMO-like variations, which may be partly forced by decadal changes in external forcing, also favors increased duration, extent and intensity of the recent European heatwaves through increasing the duration, zonal width, slow decay and quasi-stationarity of the EB or UB event. Their joint effect strongly contributed to the recent increases in the frequency, extent and intensity of European heat waves.

Data Availability Statement

The E-OBS daily gridded land-only observational data set (Cornes et al., 2018) is taken from the website (https://www.ecad.eu/download/ensembles/download.php). The ERA5 reanalysis data (Hersbach et al., 2020) is taken from the website (https://climate.copernicus.eu/climate-reanalysis). The AMO index (Enfield et al., 2001) is available online (https://psl.noaa.gov/data/timeseries/AMO/). The daily NAO index from (https://www.cpc.ncep.noaa.gov/products/precip/CWlink/pna/nao.shtml). The monthly SST data were taken from the Hadley Centre HadISST (Rayner et al., 2003) website (https://www.metoffice.gov.uk/hadobs/index.html). The CMIP6 models data (Eyring et al., 2016) from the website (https://esgf-node.llnl.gov/search/cmip6/). All codes used in the present study are available from the corresponding author on request. The Climate Data Toolbox for MatlabR2018a software (Greene et al., 2019) is used for plotting and the NCAR Command Language (Version 6.6.2) software is used for plotting Figure 2.

Acknowledgments
This research was supported by the National Natural Science Foundation of China (Grants 42150204, 42288101, 41975068, and 42075025), China Postdoctoral Science Foundation (2023M730279), and the Beijing Normal University Talent Introduction Project of China (12807-312232101).

References

Barriopedro, D., Fischer, E. M., Luterbacher, J., Trigo, R. M., & Garcia-Herrera, R. (2011). The hot summer of 2010: Redrawing the temperature record map of Europe. *Science*, *332*(6026), 220–224. https://doi.org/10.1126/science.1201224

Black, E., Blackburn, M., Harrison, G., Hoskins, B., & Methven, J. (2004). Factors contributing to the summer 2003 European heatwave. *Weather*, *59*(8), 218–223. https://doi.org/10.1256/wea.74.04

Black, E., & Sutton, R. (2007). The influence of oceanic conditions on the hot European summer of 2003. *Climate Dynamics*, *28*(1), 53–66. https://doi.org/10.1007/s00382-006-0179-8

Cornes, R., van der Schrier, G., van den Besselaar, E. J. M., & Jones, P. (2018). An ensemble version of the E-OBS temperature and precipitation datasets [Dataset]. Journal of Geophysical Research: Atmospheres, *123*(17), 9391–9409. https://doi.org/10.1029/2017JD028200

Dai, A., & Bloecker, C. E. (2019). Impacts of internal variability on temperature and precipitation trends in large ensemble simulations by two climate models. *Climate Dynamics*, *52*(1–2), 289–306. https://doi.org/10.1007/s00382-018-4132-4

Dai, A., Fyfe, J. C., Xie, S.-P., & Dai, X. (2015). Decadal modulation of global surface temperature by internal climate variability. *Nature Climate Change*, *5*(6), 555–559. https://doi.org/10.1038/nclimate2605

Della-Marta, P. M., Luterbacher, J., von Weissenfluh, H., Xoplaki, E., Brunet, M., & Wanner, H. (2007). Summer heat waves over western Europe 1880–2003, their relationship to large-scale forcings and predictability. *Climate Dynamics*, *29*(2–3), 251–275. https://doi.org/10.1007/s00382-007-0233-1

Dole, R., Hoerling, M., Perlwitz, J., Eischeid, J., Pegion, P., Zhang, T., et al. (2011). Was there a basis for anticipating the 2010 Russian heat wave? *Geophysical Research Letters*, *38*(6), L06702. https://doi.org/10.1029/2010GL046582

Duchez, A., Frajka-Williams, E., Josey, S. A., Evans, D. G., Grist, J. P., Marsh, R., et al. (2016). Drivers of exceptionally cold North Atlantic Ocean temperatures and their link to the 2015 European heat wave. *Environmental Research Letters*, *11*(7), 074004. https://doi.org/10.1088/1748-9326/11/7/074004

Enfield, D. B., Mestas-Nunez, A. M., & Trimble, P. J. (2001). The Atlantic Multidecadal Oscillation and its relationship to rainfall and river flows in the continental U.S. [Dataset]. Geophysical Research Letters, *28*(10), 2077–2080. https://doi.org/10.1029/2000GL012745

Eyring, V., Bony, S., Meehl, G. A., Senior, C. A., Stevens, B., Stouffer, R. J., & Taylor, K. E. (2016). Overview of the coupled model Intercomparison project phase 6 (CMIP6) experimental design and organization [Dataset]. Geoscientific Model Development, *9*(5), 1937–1958. https://doi.org/10.5194/gmd-9-1937-2016

Fischer, E. M., & Schar, C. (2010). Consistent geographical patterns of changes in high-impact European heatwaves. *Nature Geoscience*, *3*(6), 398–403. https://doi.org/10.1038/ngeo866

Fischer, E. M., Seneviratne, S. I., Vidale, P. L., Luthi, D., & Schär, C. (2007). Soil moisture–atmosphere interactions during the 2003 European summer heat wave. *Journal of Climate*, *20*, 5081–5099. https://doi.org/10.1175/JCLI4288.1

Folland, C. K., Knight, J., Linderholm, H. W., Fereday, D., Ineson, S., & Hurrell, J. W. (2009). The summer North Atlantic Oscillation: Past, present and future. *Journal of Climate*, *22*(5), 1082–1103. https://doi.org/10.1175/2008JCLI2459.1

Franzke, C. L. E. (2014). Nonlinear climate change. *Nature Climate Change*, *4*(6), 423–424. https://doi.org/10.1038/nclimate2245

Ghosh, R., Muller, W. A., Eichhorn, A., Baehr, J., & Bader, J. (2019). Atmospheric pathway between Atlantic multidecadal variability and European summer temperature in the atmospheric general circulation model ECHAM6. *Climate Dynamics*, *53*(1–2), 209–224. https://doi.org/10.1007/s00382-018-4578-4

Greene, C. A., Thirumalai, K., Kearney, K. A., Delgado, J. M., Schwanghart, W., Wolfenbarger, N. S., et al. (2019). The climate data toolbox for MATLAB. *Geochemistry, Geophysics, Geosystems*, *20*, 3774–3781. https://doi.org/10.1029/2019GC008392

Hall, R. J., Jones, J. M., Hanna, E., Scaife, A. A., & Erdelyi, R. (2017). Drivers and potential predictability of summer time North Atlantic polar front jet variability. *Climate Dynamics*, *48*(11–12), 3869–3887. https://doi.org/10.1007/s00382-016-3307-0

Hersbach, H., Bell, B., Berrisford, P., Hirahara, S., Horányi, A., Muñoz-Sabater, J., et al. (2020). The ERA5 global reanalysis [Dataset]. Quarterly Journal of the Royal Meteorological Society, *146*(730), 1999–2049. https://doi.org/10.1002/qj.3803

Ionita, M., Nagavciuc, V., Kumar, R., & Rakovec, O. (2020). On the curious case of the recent decade, mid-spring precipitation deficit in central Europe. *npj-Climate and Atmospheric Science*, *3*(1), 49. https://doi.org/10.1038/s41612-020-00153-8

Johnson, N. C., Xie, S., Kosaka, Y., & Li, X. (2018). Increasing occurrence of cold and warm extremes during the recent global warming slowdown. *Nature Communications*, *9*(1), 1724. https://doi.org/10.1038/s41467-018-04040-y

Li, M., Yao, Y., Simmonds, I., Luo, D., Zhong, L., & Chen, X. (2020). Collaborative impact of the NAO and atmospheric blocking on European heatwaves, with a focus on the hot summer of 2018. *Environmental Research Letters*, *15*(11), 114003. https://doi.org/10.1088/1748-9326/aba6ad

Liu, A., Huang, Y., & Huang, D. (2022). Inter-model spread of the simulated winter surface air temperature over the Eurasian continent and the physical linkage to the jet streams from the CMIP6 models. *Journal of Geophysical Research: Atmospheres*, *127*(22), e2022JD037172. https://doi.org/10.1029/2022JD037172

Luo, B., Luo, D., Wu, L., Zhong, L., & Simmonds, I. (2017). Atmospheric circulation patterns which promote winter Arctic sea ice decline. *Environmental Research Letters*, *12*(5), 054017. https://doi.org/10.1088/1748-9326/aa69d0

Luo, D., Chen, X., & Feldstein, F. (2018). Linear and nonlinear dynamics of North Atlantic Oscillations: A new thinking of symmetry breaking. *Journal of the Atmospheric Sciences*, *75*(6), 1955–1977. https://doi.org/10.1175/JAS-D-17-0274.1

Luo, D., Yao, Y., & Dai, A. (2015). Decadal relation between European blocking and North Atlantic Oscillation during 1978–2011. Part I: Atlantic conditions. *Journal of the Atmospheric Sciences*, *72*(3), 1152–1173. https://doi.org/10.1175/JAS-D-14-0039.1

Luo, D., Zhang, W., Zhong, L., & Dai, A. (2019). A nonlinear theory of atmospheric blocking: A potential vorticity gradient view. *Journal of the Atmospheric Sciences*, *76*(8), 2399–2427. https://doi.org/10.1175/JAS-D-18-0324.1

Mecking, J. V., Drijfhout, S. S., Hirschi, J. J., & Blaker, A. T. (2019). Ocean and atmosphere influence on the 2015 European heatwave. *Environmental Research Letters*, *14*(11), 114035. https://doi.org/10.1088/1748-9326/ab4d33

Meehl, G. A., & Tebaldi, C. (2004). More intense, more frequent, and longer lasting heat waves in the 21st century. *Science*, *305*(5686), 994–997. https://doi.org/10.1126/science.1098704

O'Reilly, C. H., Woollings, T., & Zanna, L. (2017). The dynamical influence of the Atlantic Multidecadal Oscillation on continental climate. *Journal of Climate*, *30*(18), 7213–7230. https://doi.org/10.1175/JCLI-D-16-0345.1

Qin, M., Dai, A., & Hua, W. (2020). Quantifying contributions of internal variability and external forcing to Atlantic multidecadal variability since 1870. *Geophysical Research Letters*, *47*(22), e2020GL089504. https://doi.org/10.1029/2020GL089504

Rayner, N. A., Parker, D. E., Horton, E. B., Folland, C. K., Alexander, L. V., Rowell, D. P., et al. (2003). Global analyses of sea surface temperature, sea ice, and night marine air temperature since the late nineteenth century [Dataset]. Journal of Geophysical Research: Atmospheres, *108*(D14), 4407. https://doi.org/10.1029/2002JD002670

Rousi, E., Kornhuber, K., Beobide-Arsuaga, G., Luo, F., & Coumou, D. (2022). Accelerated Western European heatwave trends linked to more-persistent double jets over Eurasia. *Nature Communications*, *13*(1), 3851. https://doi.org/10.1038/s41467-022-31432-y

Rousi, E., Selten, F., Rahmstorf, S., & Coumou, D. (2021). Changes in North Atlantic atmospheric circulation in a warmer climate favor winter flooding and summer drought over Europe. *Journal of Climate*, *34*(6), 2277–2295. https://doi.org/10.1175/JCLI-D-20-0311.1

Schaer, C., Vidale, P. L., Lüthi, D., Frei, C., Haberli, C., Liniger, M. A., & Appenzeller, C. (2004). The role of increasing temperature variability in European summer heatwaves. *Nature*, *427*(6972), 332–336. https://doi.org/10.1038/nature02300

Schneidereit, A., Schubert, S., Vargin, P., Lunkeit, F., Zhu, X., Peters, D. H. W., & Fraedrich, K. (2012). Large-scale flow and the long-lasting blocking high over Russia: Summer 2010. *Monthly Weather Review*, *140*(9), 2967–2981. https://doi.org/10.1175/MWR-D-11-00249.1

Schoetter, R., Cattiaux, J., & Douvill, H. (2015). Changes of western European heat wave characteristics projected by the CMIP5 ensemble. *Climate Dynamics*, *45*(5–6), 1601–1616. https://doi.org/10.1007/s00382-014-2434-8

Simpson, I. R., Bacmeister, J., Neale, R. B., Hannay, C., Gettelman, A., Garcia, R. R., et al. (2020). An evaluation of the large-scale atmospheric circulation and its variability in CESM2 and other CMIP models. *Journal of Geophysical Research*, *125*(13), e2020JD032835. https://doi.org/10.1029/2020JD032835

Stefanon, M., D'andera, F., & Drobinski, P. (2012). Heatwave classification over Europe and the mediterranean region. *Environmental Research Letters*, *7*(1), 014023. https://doi.org/10.1088/1748-9326/7/1/014023

Stott, P. A. (2003). Attribution of regional-scale temperature changes to anthropogenic and natural causes. *Geophysical Research Letters*, *30*(14), 1728. https://doi.org/10.1029/2003GL017324

Stott, P. A., Stone, D. A., & Allen, M. R. (2004). Human contribution to the European heatwave of 2003. *Nature*, *432*(7017), 610–614. https://doi.org/10.1038/nature03089

Sutton, R. T., & Hodson, D. L. (2005). Atlantic Ocean forcing of North American and European summer climate. *Science*, *309*(5731), 115–118. https://doi.org/10.1126/science.1109496

Tibaldi, S., & Molteni, F. (1990). On the operational predictability of blocking. *Tellus*, *42A*(3), 343–365. https://doi.org/10.1034/j.1600-0870.1990.t01-2-00003.x

Trigo, R. M., Garcia-Herrera, R., Diaz, J., Trigo, I. F., & Valente, M. A. (2005). How exceptional was the early August 2003 heatwave in France. *Geophysical Research Letters*, *32*(10), L10701. https://doi.org/10.1029/2005GL022410

Vandentorren, S., Suzan, F., Medina, S., Pascal, M., Maulpoix, A., Cohen, J. C., & Ledrans, M. (2004). Mortality in 13 French cities during the August 2003 heat wave. *American Journal of Public Health*, *94*(9), 1518–1520. https://doi.org/10.2105/AJPH.94.9.1518

Van Oldenborgh, G. J., Wehner, M. F., Vautard, R., Otto, F. E. L., Seneviratne, S. I., Stott, P. A., et al. (2022). Attributing and projecting heatwaves is hard: We can do better. *Earth's Future*, *10*(6), e2021EF002271. https://doi.org/10.1029/2021EF002271

Vautard, R., Yiou, P., D'Andrea, F., de Noblet, N., Viovy, N., Cassou, C., et al. (2007). Summertime European heat and drought waves induced by wintertime rainfall deficit. *Geophysical Research Letters*, *34*(7), L07711. https://doi.org/10.1029/2006GL028001

Wang, H., & Luo, D. (2020). Summer Russian heat waves and their links to Greenland ice melting and sea surface temperature anomalies over North Atlantic and Barents-Kara Seas. *Environmental Research Letters*, *15*(11), 114048. https://doi.org/10.1088/1748-9326/abbd03

Wilks, D. S. (2011). *Statistical methods in the atmospheric sciences* (3rd ed.). Academic Press.

Wilks, D. S. (2016). The stippling shows statistically significant grid points: How research results are routinely overstated and overinterpreted, and what to do about it. *Bulletin of the American Meteorological Society*, *97*(12), 2263–2273. https://doi.org/10.1175/BAMS-D-15-00267.1

Witze, A. (2022). Extreme heatwaves: Surprising lessons from the record warmth. *Nature*, *608*(7923), 464–465. https://doi.org/10.1038/d41586-022-02114-y

Wyser, K., Kjellström, E., Koenigk, T., Martins, H., & Döscher, R. (2020). Warmer climate projections in EC-Earth3-veg: The role of changes in the greenhouse gas concentrations from CMIP5 to CMIP6. *Environmental Research Letters*, *15*(5), 054020. https://doi.org/10.1088/1748-9326/ab81c2

Yao, Y., & Luo, D. (2015). Do European blocking events precede North Atlantic Oscillation events? *Advances in Atmospheric Sciences*, *32*(8), 1106–1118. https://doi.org/10.1007/s00376-015-4209-5

Zhang, R., Sun, C., Zhu, J., Zhang, R. H., & Li, W. (2020). Increased European heat waves in recent decades in response to shrinking Arctic sea ice and Eurasian snow cover. *NPJ Climate and Atmospheric Science*, *3*(1), 7. https://doi.org/10.1038/s41612-020-0110-8

Erratum

The originally published article contained a typographical error. In the second sentence of the second paragraph of Section 2.4, "$\Delta = -5°, 0°, 5°$" has been corrected to read "$\Delta = -4°, 0°, 4°$." This may be considered the authoritative version of record.